Cationic Nanogel Carriers for siRNA delivery to the Posterior Segment of the Eye

Cationic Nanogel Carriers for siRNA delivery to the Posterior Segment of the Eye

By

Cheryl Bachan

H.B.Sc.

A Thesis

Submitted to the School of Graduate Studies

In Partial Fulfillment of the Requirements

For the Degree of Master of Applied Science

McMaster University

Descriptive Note

McMaster University, Hamilton ON

MASTER OF APPLIED SCIENCE (2016) Hamilton, Ontario (Biomedical Engineering)

TITLE: Cationic Nanogel Carriers for siRNA delivery to the Posterior Segment of the Eye

AUTHOR: Cheryl P. Bachan, H.B.Sc. (University of Ottawa)

SUPERVISOR: Dr. Heather Sheardown

NUMBER OF PAGES: i, 60

ABSTRACT

Current treatment for posterior segment ocular diseases requires intravitreal injections administered every 4-6 weeks. The potential for siRNA to be used to treat these diseases is extremely attractive due to the specificity of these molecules and their potential for making long term changes to the expression patterns of the cells. Due to physiological recognition, however siRNA undergoes rapid degradation upon application. The development of cationic nanogels using polymeric "smart" biomaterials with degradable components to transport siRNA is described. pH – sensitive N, N dimethylaminoethyl methacrylate (DMAEMA) was crosslinked with thermo-sensitive diethylene glycol methacrylate (DEGMA), by free radical emulsion-precipitation polymerization. Size, charge and morphology were analyzed to assess potential as a nanovehicle. Through modification of the particle composition, cationic nanogels, determined by zeta potential, with sizes of approximately 160 nm confirmed with dynamic light scattering (DLS), were synthesized. A composition of 55:45 (DEGMA:DMAEMA); a size and charge ideal for cellular uptake. These particles had minimal impact on cell proliferation and exhibited spherical morphology when imaged by TEM at physiological pH. The structure was maintained between pH 3.5-9. Sensitivity to pH was shown by DLS through swelling at physiological pH, which may be useful can be taken advantage of in future studies for loading and release.

Degradation with a reducing agent was shown using gel permeation chromatography, DLS and turbidity analysis. The results suggest this formula will

undergo degradation in the cell. Reducing environments mimicking intracellular conditions that promoted degradation of the crosslinker showed enhanced release of dexamethasone phosphate as a model drug. Ongoing work is focused on examining gene silencing using these formulations.

ACKNOWLEDGEMENTS

First of all thank you to Heather for accepting me into her lab and all the opportunities that came along with it. Truly a no limits environment, I was able to explore and to present my work in a variety of forums which I would have never been exposed to in a different setting. Heather's advice throughout my project and guidance throughout, built my confidence in my research and helped me shape my future goals. Thank you to Todd Hoare for assisting in the start of my wet-lab experience in chemical engineering and allowing me space in his lab when I was first starting. I appreciated your suggestions and encouragement throughout my project.

A huge thank you to Megan Dodd, who not only became a very dear friend, but was a great help in *in vitro* studies as well as my motivation throughout. Thank you for the train trips and talks that have helped me gain confidence in my abilities in research. I am lucky to have made labmates/friends who have let me sleep over through long lab nights (Alysha) and steal their office space (Vida/Myrto/Fei).I'm grateful to the Sheardown lab group, the Hoare lab neighbours, and the friends I've made who have made me laugh at foil ice trays and melted transfer pipettes. Travelling with you all has made this experience that much more special. Thank you to those that discussed ideas with me, showed me their protocols and accompanied me for stress-relieving excursions (Nicole, Madeline and Emilia). I never thought I'd make so many meaningful relationships in such a short period of time and find in Alysha a labmate that became so close through our shared mentality of over stressing. I'm very grateful to have met you as we think the same, share each others' highs and lows, and keep each other moving forward. So grateful to have had as you as a bridesmaid and a friend. After all the hospital trips and personal life chaos for the last two years I've been very lucky to be able to share this with you and receive love and support. I'll continue to be there for you as well!

But most of all my family has been the backbone of my journey. Huge thanks to my parents who never lose their faith in me and see things inside me I cannot fathom. It's been a rocky road, thank you for being by my side even when we were far apart. Alexei- my husband, thank you for letting me put school before us, for unwaivering support and love. For understanding that I'd rather spend time in the lab on holidays, rather than sit at home wanting to figure something out and ruin our time together, for letting me put school ahead of wedding planning as a priority, and most of all for understanding after having a beautiful wedding weekend that I wanted to get back to work, even though I had the option to take time off. I can't wait to spend time and finally honeymoon together. I love you. And to my furbaby Sneg, nothing beats coming home after a stressful day to the happiest face in the world.

TABLE OF CONTENTS

LIST OF FIGURES

LIST OF TABLES

LIST OF ABBREVIATIONS

MWCO	Molecular weight cut off
DLS	Dynamic light scattering
TEM	Transmission electron microscopy
NMR	Nuclear magnetic resonance
MTT	3-(4,5-Dimethylthiazol-2-Yl)-2,5-Diphenyltetrazolium Bromide
DMAEMA	Dimethyl amino ethyl methacrylate
DEGMA	Diethylene glycol methacrylate
CTAB	Cetyl trimethylammonium bromide
PBS	Phosphate buffered saline
TLC	Thin layer chromatography
UV	Ultraviolet
TCEP	Tris(2-carboxyethyl)phosphine
HPLC	High performance liquid chromatography
GPC	Gel permeation chromatography
LCST	Lower critical solution temperature
DMSO	Dimethyl sulfoxide
HEPES	4-(2-hydroxyethyl)-1-piperazineethanesulfonic acid
DXP	Dexamethasone phosphate
LC	Loading capacity
siRNA	Silencing ribonucleic acid
NG	Nanogel

DMEM	Dulbecco's modified eagle medium
CTAB	Cetyl trimethylammonium bromide
TEM	Transmission electron microscopy
DNA	Deoxyribonucleic acid
GFP	Green fluorescence protein
RPE	Retinal epithelial
BRB	Blood retinal barrier
AMD	Age-related macular degeneration
VEGF	Vascular endothelial growth factor
RNA	Ribonucleic acid
RISC	RNA-induced silencing complex
mRNA	Messenger ribonucleic acid

Chapter 1. INTRODUCTION

Current posterior ocular delivery systems require painful injections of drugs or inhibitors every four weeks. This increases the potential for inflammation, patient discomfort and cost (Mousa *et al*., 2010). These injections may decrease symptoms of ocular neovascular diseases but there is room for improvement due to the financial impact and associated side effects. Clinical data support the delivery of siRNA targetting angiogenic growth factors for posterior eye diseases resulting from choroidal neovascularization (Guzman-Aranguez *et al*., 2013). siRNA, when delivered via injection, requires high doses as a significant amount degrades extracellularly, prior to intracellular recognition where it readily undergoes its mechanism of action (Deng *et al*., 2014; Kennedy *et al*., 2004). Its overall negative charge decreases potential for cell entry due to electrostatic repulsion from the cell's negatively charged cellular membrane and even with local injections have been shown to have less than 1% or siRNA delivered reach its' target (Xia *et al*., 2004). To enhance cellular penetration, decrease doses and costs associated, nanoparticles provide an attractive alternative for the delivery of siRNA.

Particles that have a diameter of 10nm-1000nm are considered nanoparticles (Bucolo *et al*., 2012). Cellular entry by endocytosis of polymeric nanovehicles, are largely governed by physicochemical properties. Spherical nanoparticles have been shown to readily enter the cell within the size range of 50nm-200nm (Yin Win & Feng, 2005). These sizes enhance cellular uptake and decrease potential for immune response (Sultana *et al*., 2013). Electrostatically favourable interactions enhance cell entry when the nanoparticle is cationic. Cationic nanoparticles serve as an ideal siRNA carrier as they

are hydrophilic and would electrostatically bind and deliver this therapeutic. Cellular endocytosis would also be electrostatically enhanced due to its negative surface charge.

Nanogels were investigated in this project due to the common biologically favourable characteristics they possess such as elasticity, highly hydrated networks and reduced protein adsorption (Raemdonck *et al*., 2009). This particular type of nanoparticle is termed as a nanogel as it is a nano-sized hydrogels that are made of a crosslinked polymer network that have the ability to absorb a large quantity of water (Peppas *et al*., 2000). These crosslinked networks can either be established through chemical bonds or physical interactions (Hennink & van Nostrum, 2002). Common approaches to produce these types of gels are through emulsion or precipitation polymerization (Landfester, 2006; Pelton, 2000). When synthesized with biomaterials, there is high potential for polymeric degradation within the cell (Azevedo & Reis, 2004). "Smart" biomaterials further enhance the potential of the nanogels through stimuli responsive behaviour and will be investigated through this study (Dorwal, 2012). This could enhance tunability of therapeutic loading conditions and release profiles.

These hydrophilic particles show excellent promise for enhanced delivery of gene therapeutics when there is a cationic charge density. Taken together with their potential for degradation and cytocompatability, polymeric cationic nanogel synthesis for siRNA delivery as an attractive area of research.

1.1 Research Objectives

The main purpose of this research was to develop novel cationic nanogels using biodegradable components. To achieve this, the first objective was to synthesize a degradable crosslinker which could be combined with appropriate combinations of biologically acceptable materials to generate nanogels. The second objective was to then create variable compositions of particles of nano-size and cationic charge. Evaluation of the degradability, physiological stability and cytotoxicity of these gels was investigated to ensure the vehicles had potential as biological nano carriers. To assess potential for use as a transfection reagent, model drug loading and release and siRNA delivery through transfection studies were pursed.

1.2 Thesis Outline

This thesis has been divided into five chapters. Chapter 1 provides an introduction to the body of work presented and outlines the research objectives. Chapter 2 provides an overview of the relevant literature. Chapter 3 describes the materials, the synthesis procedures and the characterization techniques and protocols. The results and discussion can be found in Chapter 4. An analysis of the data as it relates to the objectives is presented. Chapter 5 concludes the thesis work and suggests research directions for future studies.

Chapter 2. LITERATURE REVIEW

2.1 Eye anatomy and physiological challenges to posterior therapeutic ocular delivery

Anatomically, the eye can be divided into sections, the anterior and posterior segment. The posterior segment makes up nearly 2/3 of the eye volume and consists mainly of the vitreous humour, choroid, sclera, retina and optic nerve (Kiel, 2010, Figure 2.1). Three concentric layers comprised of the external fibrous layer including the cornea and sclera, middle vascular layer that contains the ciliary body and the choroid and the innermost neural layer made by the retina exist in this small, globe-like structure (DelMonte & Kim, 2011). Posterior drug delivery requires passing through these layers to reach targets in the retina.

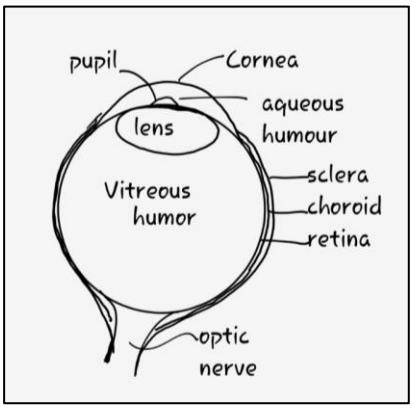

Figure 2.1 Basic anatomy of the eye.

The outer epithelial layers are comprised of intercellular tight junctions that impede transport of hydrophobic molecules (DelMonte & Kim, 2011). The middle vascular layer is made of the choroid which contains the ocular vasculature that provides

routes of drug entry and removal from the eye (Tokayer, Jia, Dhalla, & Huang, 2013). This layer does not present much of a barrier for hydrophilic small molecules such as gene therapeutics; however this system promotes systemic circulation impeding the target retinal penetration (Lutty *et al*., 2010). The retina is the innermost of these three layers and contains the neural network that sends signals through the optic nerve to the brain. This layer provides significant barriers to transport of the drug therapeutic to the retina (Kwatra, 2013).

Therapeutic delivery of active agents to the posterior segment is severely impeded by the blood-retinal-barrier that is comprised of the retinal vascular endothelium and the retinal pigment epithelium. The highly packed nature of the retinal pigment epithelial (RPE) cells and the tight junctions between them prevents uptake of most therapeutics, decreasing transport of even water soluble molecules and drugs (Runkle & Antonetti, 2011). The inner layer receives nourishment from the epithelium to the rods and cones that receive light and transport electrical signals to the optic nerve. This barrier of two types of tightly aligned cells act as a significant obstacle to non-invasive drug administration routes and limits posterior delivery to mainly intravitreal injections.

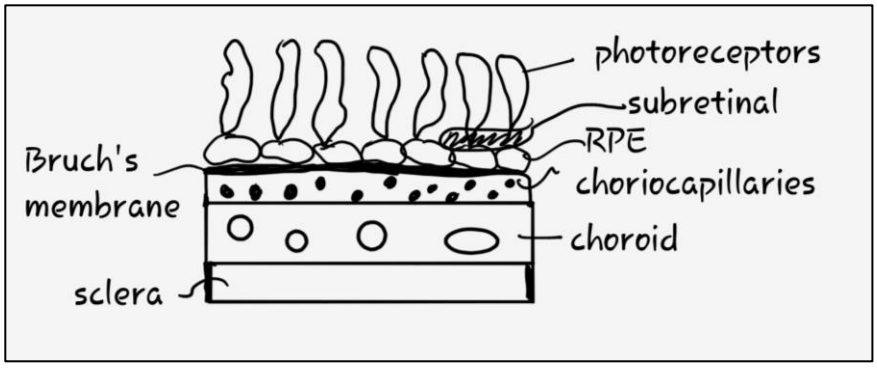

Figure 2.2 Schematic of RPE cell layers in the retina

Posterior segment delivery is impeded from the anterior segment due to the high turnover rate of the tear film and aqueous humour (Del Amo & Urtti, 2008). To penetrate to the back of the eye requires high concentrations, hydrophobic character and ability to overcome the physical barrier of the lens (Rajendran, Knölker, & Simons, 2010). Systemic delivery is a challenge as it requires both a targeted approach at high drug concentrations to overcome the retinal barrier which increases the cost of this technology and potential cytotoxicity. High concentrations are key as less than 1% of therapeutics delivered has the ability to traverse the blood-retinal-barrier (Duvvuri, Majumdar, & Mitra, 2003). Since high concentrations of drug, which can be cytotoxic, are required to reach therapeutic levels for ocular deliver, targeted therapies of physiologically recognized therapeutics such as siRNA delivery are favoured and have immense potential as a treatment modality.

Intravitreal injections, although the main treatment option for posterior eye segment, are inefficient routes of delivery as much of the delivered therapeutic is drained from the vitreous through the trabecular meshwork and systemically through the vascular

layer of the blood retinal barrier (BRB) (Geroski & Edelhauser, 2000). This procedure also increases risk for infection due to the need for frequent injections in addition to a number of other side effects such as retinal detachment and hemorrhages (Geroski & Edelhauser, 2000). Increasing bioavailability will be accompanied by less frequent subretinal injections. This targeted injection delivers therapeutics directly to the retina, decreasing doses from loss of therapeutic through drainage routes or degradation and costs associated with intravitreal injections (Wert, Skeie, Davis, Tsang, & Mahajan, 2012). Regardless of administration route, the BRB prevents treatment of degenerative retinal diseases such as age-related macular degeneration using non-invasive options.

Drug/gene delivery is further impeded by the effective drainage system of the eye. This organ has several routes to effectively remove drugs. These routes are highly efficient at rapidly clearing foreign bodies and protecting the intraocular environment (Del Amo & Urtti, 2008). Due to these biological safeguards, delivery of therapeutics at an effective dose is a challenge and increases cost and difficulty of treatment.

2.2 Wet-Age Related Macular Degeneration

Age-related macular degeneration is an eye disease of the posterior segment. It is the leading cause of irreversible blindness in the developed world (Alexandru & Alexandra, 2016). The prominence of this disease increases need for development of treatments with higher efficiency. This will both benefit healthcare costs and decrease the incidence of side effects and as well as increasing patient acceptability. Diagnosis of AMD typically comes due to the loss of central vision, where the macula is located, in the

posterior region of the retina. This small central region controls visual acuity. Damage to this part of the eye results in central vision loss (Alexandru & Alexandra, 2016).

As we age the Bruch's membrane, the inner most layer of the choroid, gets thicker and can form drusen (Guymer, Luthert, & Bird, 1999). Together with inflammation and neovascularization in the choroid, they serve as indicators of "wet" age-related macular degeneration. Neovascularization is the rapid formation of new blood vessels and, in the case of wet-AMD, these new blood vessels are poorly formed and leak both blood and fluid, causing damage to the Bruch's membrane, the outer layer of the choroid (Klein *et al., 2008).* The destruction of the architecture of the Bruch's membrane, damages the macular area of the retina (Pauleikhoff, Harper, Marshall, & Bird, 1990).

Patients become aware of their condition either from central vision loss or diagnosis through posterior eye exams that look at the vasculature and signs of drusen, a hallmark of the dry AMD, which always precedes the wet form. The presence of drusen (small deposits in the retina), inflammation and choroidal neovascularization lead to a positive diagnosis (Klein *et al*., 2008). Since wet-AMD is irreversible, early diagnosis is pertinent in identifying a treatment plan and regaining control of new blood vessel growth through drug/gene therapy.

Wet-AMD development is suggested to be caused by genetic variants and/or oxygen deprivation that trigger RPE cells to synthesize vascular endothelial growth factor (VEGF) (Tuo, Bojanowski, & Chan, 2004). This growth factor induces new blood vessel growth and is often expressed when there is damage, blocked vessels or during embryonic

development (Storkebaum, Lambrechts, & Carmeliet, 2004). VEGF, when expressed at high levels during times when unneeded for specific trauma can cause the development of unnecessary blood vessels that are poorly formed and leak, destroying the retina (Bressler, 2009). Current treatment methods are limited, invasive and come with a myriad of side effects.

2.3 Administration Routes and Current Therapies

Systemic delivery of therapeutics to the back of the eye is highly impeded by the BRB described earlier. As little as 1-2% of drugs are able to cross the BRB and reach the retinal epithelial layer (Del Amo & Urtti, 2008). To increase bioavailability intravitreal injections are commonly used for anti-VEGF therapies (Geroski & Edelhauser, 2000). Drug-releasing scaffold periocular implantations have the potential for prolonged drug release. However, with this treatment, there is a need to traverse the BRB in order for the therapeutic to reach its target (Edelhauser *et al*., 2010). Typically, intravitreal injections are used to deliver the drug to its target, however the clearance mechanisms of the posterior eye mean that injections must be performed frequently, which is inconvenient for both the patient and the physician (Geroski & Edelhauser, 2000). Additionally, each injection carries with it a significant risk of secondary complications including retinal detachment, cataract formation and endophthalmitis. Less common, but showing promise for improved efficacy, are sub-retinal injections. This differs from the simpler approach by administering the drug into the subretinal space (Wert *et al*., 2012). This highly advanced and technical surgery would require more skill and cost but would increase bioavailabilty through local injections.

While blindness due to wet-AMD cannot be fully reversed, treatment has been shown in some cases to restore some vision loss. These therapies, which are administered intravitreally, reduce the effect of VEGF by administering antibodies that have high specificity for VEGF binding. Drugs on the market that undergo this mechanism include Ranibizumab (Lucentis) and Bezacizumab (Avastin) antibodies (Kovach, Schwartz, Flynn, & Scott, 2012; Schmidt-Erfurth *et al*., 2014). Aflibercept (Eyelea), uses a fusion protein that binds isoforms of VEGF to inhibit its function(Schmidt-Erfurth *et al*., 2014). The use of anti-VEGF treatments, while effective, have been shown to have rare, but severe side effects. The most prominent being the instigation of thromboembolic events such as stroke or haemorrhage. VEGF expression stimulates angiogenesis, but once this response has been triggered and subsequently inhibited, these cells can be prone thrombosis (Kilickap, 2003). Furthermore, VEGF inhibition has also been shown to decrease the regenerative ability of endothelial cells and promote coagulation mechanisms. These potential side effects and frequent dosages of 4-6 weeks that encourages coagulation processes, have led to research for better treatment options. Bevasiranib, an siRNA injection has shown potential for vast increase between drug administration from 4 weeks to 12 weeks in clinical trials (Mousa *et al*., 2010). While not suggested as a therapy on its own, improvement can be made by protecting this highly effective siRNA with a nanoparticle carrier.

2.4 siRNA delivery and mechanism of action

siRNA are short double stranded fragments of RNA, ranging in length from 19 to 25 base pairs, that trigger RNA interference. This is a conserved process that allows for

gene silencing pre-translationally of target mRNA (Reischl & Zimmer, 2009). They have a negatively charged phosphate backbone and are easily recognized by intracellular protein complexes (Pham & Sontheimer, 2005). Delivery of appropriate siRNA to the retinal pigment epithelium will decrease production of VEGF as RPE cells express these growth factors in high quantity in cases of wet – AMD (Storkebaum *et al*., 2004). siRNA delivery is an attractive method, as it is a compound that is physiologically recognized and once endocytosed by the cell rapidly undergoes its mechanism of action (Ohno-Matsui, Yoshida, Uetama, Mochizuki, & Morita, 2003; Pham & Sontheimer, 2005). Upon entry into mammalian cells siRNA is phosphorylated where it is recognized in the cytoplasm by RNA inducing silencing complexes (RISC). This complex is composed of many proteins that serve to enhance binding of siRNA and cleave target mRNA. An enzyme called Dicer works first to create single stranded 21 nucleotide fragments from the double stranded siRNA and binds this antisense single strand with the assistance of Argonaute 2, a protein that enhances binding to the complex and cleavage of target mRNA (Watts, Deleavey, & Damha, 2008; Zamore, Tuschl, Sharp, & Bartel, 2000). Other proteins are then recruited to enhance interactions and mechanism for target mRNA cleavage. This complex will then recruit the target mRNA containing the genetic material of undesired protein production and bind it within the RISC complex if the strands are complementary (Hammond, Bernstein, Beach, & Hannon, 2000). The target mRNA is then degraded and the process is repeated more than 100 times.

siRNA are highly effective as they are easily recognized within the cell. They can be designed to be highly specific but undergo rapid extracellular degradation (Deng *et al*.,

2014). They are recognized by plasma nucleases and must be delivered locally to avoid degradation prior to reaching their target (Xia *et al*., 2004). Even through local injections like the eye, the effect has been minimal and there is still a requirement for enhanced cellular penetration for siRNA to perform to its maximum potential (Check, 2005).

2.5 Vectors for enhancement of siRNA delivery

Endocytosis of naked siRNA is limited due to unfavourable interactions with the negatively charged cellular membrane. siRNA has a phosphate backbone which imparts a an overall negative charge, therefore undergoing repulsion through surface interactions with the cell (Reischl & Zimmer, 2009). Its action is further limited due to recognition in the extracellular environment by endo and exonucleases that readily degrade RNA (Kennedy *et al*., 2004). While modified siRNA can be synthesized to enhance effectiveness, it still is a highly limited technology on its own. siRNA can trigger unfavourable immune responses by binding to toll-like receptors on immune cells (Fulmer, 2009). Nanoparticles are a potential solution due to their efficacy in both protecting cargo from degradation extracelluarly, and increasing cellular uptake (Raemdonck *et al*., 2009). Nanoparticles have been widely used in cancer therapies and, when loaded with siRNA, improve cellular penetration of the gene therapeutic.

Adeno-associated viruses or lentiviruses have been explored as potential vehicles for transporting siRNA across the cellular membrane. While an effective method for transfection, this delivery method can trigger antiviral immune responses in some cases. Furthermore, the loading capacity is low. In theory, these viruses show promise due to

their ability to transfect cells but risk integration with the host genome, leading to mutagenesis (HÃbel *et al*., 2010). Issues with host responses and recognition consequences render this technology impractical *in vivo*. Synthetic alternatives such as nanocarriers have been researched to avoid these intrinsic issues with viral vectors and increase tenability.

The use of nanocarriers for the delivery of genetic material allows for the control of material properties, the ability to tether targeting moieties and carry with it a reduced risk of immune response. Liposomes are phospolipid based vehicles that form micelles, hiding their hydrophobic tails in the centre under aqueous conditions to conserve energy (Hughes, Yadava, & Mesaros, 2010). They allow for delivery in most cell types, but have low shelf-life and stability. Cationic polymer based vehicles have shown enhanced endocytosis due to the favoured electrostatic interaction with the negatively charged cellular membrane and have longer shelf-lives than lipid based delivery vehicles. These nanocarriers have the potential to induce the proton sponge effect, where, once endocytosed, they increase the pH within the endosome and destroy its membrane resulting in the release of the nanovehicle into the cytoplasm (Boussif *et al*., 1995). This is essential for siRNA recognition and mechanism in the cytoplasm. Use of biomaterials that can degrade over time is an attractive quality of polymeric nanoparticles. Protein-based nanocarriers have been shown to be effective carriers of siRNA but they lack the ability to escape the endosomes and degrade prior to entry into the cytoplasm. Highly – branched dendrimers have been synthesized and used for siRNA encapsulation but not in

ocular applications (Thakur *et al*., 2012). Dendrimer synthesis is a complicated method and not an attractive solution in a scale-up model.

Nanogels are soft particles that are highly hydrated polymeric networks with sizes on the order of nanometres. They have been suggested to have utility for siRNA encapsulation (Ayame, Morimoto, & Akiyoshi, 2008). By synthesizing the nanogels from synthetic materials, the properties of the material can be tuned to suit the specific application. Degradability and the timing for degradation can be readily incorporated into the delivery vehicle.

2.6 Materials and potential for degradation

"Smart" biomaterials were used in the synthesis of the proposed nanogel delivery system. Smart biomaterials have been defined as materials that change their properties in response to either an intracellular condition or some other stimulus. They have potential utility for the delivery of siRNA due to the fact that they will be delivered intracellularly but must release their contents inside the cell to undergo mechanism (Sultana *et al*., 2013). Therefore, tailoring the systems to favour intracellular conditions leads to a higher probability for delivery to the appropriate location.

Diethylene glycol methacrylate (DEGMA) is a commonly used degradable biomaterial that decreases protein adsorption and demonstrates temperature sensitivity (Tugulu, Silacci, Stergiopulos, & Klok, 2007). At certain temperatures, this polymer is either more or less soluble in water. Dimethyl amino ethyl methacrylate (DMAEMA), the second monomer employed in these studies is commonly used for the synthesis of

cationic biomaterials due to its positive charge at physiological pH (van de Wetering, Schuurmans-Nieuwenbroek, Hennink, & Storm, 1999). It features an amine group with a pKa of 8.9 and is protonated under physiological conditions. It has the ability to be used as either a hydrophobic or hydrophilic monomer due to this character. The positive charge introduced when it is hydrophilic has been highly employed for DNA-binding. The amine group on this monomer has potential for cytotoxicity, similar to many cationic monomers (Agashe, Dutta, Garg, & Jain, 2006). Further testing will be required to ensure the biological application of the polymers made with these characteristics.

Furthermore, DMAEMA is polyester that has the potential to degrade over several weeks under physiological conditions. Hydrolytic cleavage through ester bonds is also promoted with these two monomers in a physiological setting (Acemoglu, 2004). This is beneficial for the safe removal of injected material. In order to further facilitate degradation of the nanocarrier, 2-hydroxysulfide diacrylate was used to crosslink these materials in water. The disulphide bridge gave the potential for degradation in the body. The reductive environment of the cell promotes hydrolytic cleaveage of these thiols but is also recognized by glutathione a biological reducing agent. It acts as an electron donor in the presence of disulphide bonds and reduces them to free thiols. These hydrophilic, degradable polymers have potential to undergo bioelimination through the kidneys, renal system and liver (Deshayes & Kasko, 2013).

2.7 Precipitation polymerization to create nanogels

To create nanosized particles, precipitation polymerization principles were utilized. This requires monomers that are soluble in the solvent system. The synthesis was conducted in water. The technique of combining these monomers and crosslinking agent through this method is free radical crosslinking copolymerization (Funke, Okay, & Joos-Müller, n.d.). This polymerization method is relatively simple in comparison to other controlled polymerizations making it attractive for commercialization. Monomers, initiators, and crosslinker are soluble in the solvent, the resulting polymer has lower water solubility. The nano-precipitates that result from the polymerization, are suspended through stabilizing detergents (Zetterlund, Kagawa, & Okubo, 2008). The particle size and the polydispersity of polymer prepared can be modified through a variety of factors. Temperature, spinning rate, detergent concentration for example can be manipulated to achieve the desired parameters (Zetterlund *et al.*, 2008). This type of synthesis can be run under relatively mild conditions and is not highly sensitive to air compared unlike other controlled polymerization methods. This polymerization method is attractive for commercialization due to low solvent toxicity and costs, mild and stable reaction conditions and relative control.

2.8 Cationic nanogel enhancement of siRNA ocular delivery and suggested treatment plan

Cationic nanogel materials, shown to give better delivery of siRNA, will be prepared. siRNA is an ideal ocular treatment due to the low dosing concentration, and

therefore the low injection volumes necessary. Injection of large volumes can lead to increased intraocular pressure, which results in secondary complications such as glaucoma. The low level doses are justified by the potential to halt translation of hundreds of proteins with one single siRNA. Bevasiranib on its own did not show an effect on VEGF inhibition until after six weeks, attributed to its mechanism which based on new VEGF production compared to blocking pre-existing VEGF (Mousa *et al*., 2010). For this reason, the use of a cationic nanogel in combination with a monoclonal antibody that binds VEGF with high affinity for the first treatment round followed by or concurrently with siRNA delivery would serve as a potential treatment plan. Furthermore, the suggested route of administration would be through a subretinal injection. This therapy has the potential to increase time between injections and is worth exploring to decrease cost, increase patient comfort and compliance and increase efficacy of current treatment methods.

Chapter 3. MATERIALS & METHODS

3.1 Synthesis of DEGMA:DMAEMA nanogels

Various nanogel compositions were prepared by emulsion-precipitation crosslinked co-polymerization of diethylene glycol methyl ether methacrylate (DEGMA) and dimethylamino ethyl methacrylate (DMAEMA). All monomers were purified through columns to remove inhibitors prior to polymerization (Sigma-Aldrich). 0.2mmol cross-linking agent 2-hydroxyethyl disulfide dimethacrylate was added and the mixture was adjusted to pH 4.5 prior to addition of 0.92 mM cetrimonium bromide and sonication at 10 amps for 2 minutes (Misonix S-4000). The reaction mixture was added to 95 mL of

Milli-Q water in a two-necked round bottom flask and was purged with nitrogen, mixed with a magnetic stir bar at 250 rpm and attached to a condenser for 30 minutes. The reaction vessel was lowered into an oil bath at 90˚C and the polymerization initiated with 1mol% 2,2′-azobis(amidinopropane) dihydrochloride where the reaction proceeded under inert conditions for 3.5 hours. The reaction mixture was cooled to room temperature and transferred to Spectra/Por® 6 cellulose membrane dialysis tubing of 3.5 kD for dialysis against 4.5 L of MilliQ water with 6 cycles of fresh water every 8-10 hours. The resulting nanogel suspensions were stored at 4.4 ˚C. The synthesis is depicted in Figure 3.1

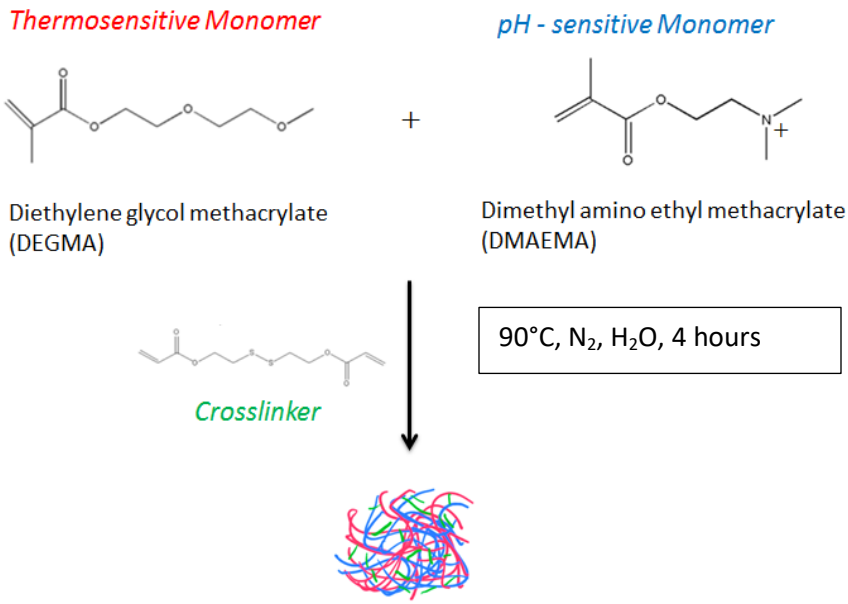

Figure 3.1 Nanogel synthesis schematic

3.2 Determination of Nanogel Concentration

Nanoparticle tracking analysis was performed with an LM 20 Nanosight to determine nanogel concentration. To calculate concentration in terms of mass, gravimetric analysis was performed on 1 mL of nanogels that were transferred to a foil

plate. Mass was recorded before and after drying at 70 ˚C. The following equation was used for gravimetric analysis.

$$\frac{(after\ drying\ mass\ of\ nanogels - mass\ of\ foil\ plate)}{/before\ drying\ mass\ of\ nanogels - mass\ of\ foil\ plate} * 100 = wt\%\ (\frac{m}{m}).$$

3.3 Size determination with dynamic light scattering

The average effective diameter was estimated with Brookhaven 90 Plus Particle Size Analyzer by dynamic light scattering with a HeNe laser and a photomultiplier tube directed at 90˚. Standard deviations were calculated over the course of 5 replicate measurements at 25˚C set to a refractive index of 1.34. Particle size distribution was calculated with the CMFT statistical method.

3.4 Zeta potential measurement for estimate of surface charge

Nanogels dissolved in 1 mM NaCl were used to assess the charge of the nanogel using the Schumolowski model for zeta potential that derives the surface charge from the electrophoretic mobility. (Zen3600 – Zetasizer Nano ZS) The prepared solution was transferred to a cuvette and a dip cell zeta probe was inserted. The system uses interferometric M3- Phase analysis light scattering to measure the electrophoretic mobility.

3.5 Transparency determination with UV spectroscopy

Transparency of nanogels was determined by adding 4.5 mg/mL of the nanogels in phosphate buffered saline into a 96-Greneir well plate. The absorbance was analyzed

spectrophotometrically at a wavelength of 500 nm. The absorbance was used in the following equation to determine transmittance.

$$\%T = 100 * 10^{-A}$$

Equation 1 Percent transmittance calculated from absorbance at 500nm. (A= Absorbance, T= Transmittance)

3.6 Potentiometric-conductometric titration for determination of DMAEMA content

Nanogels were diluted to 1 mg/mL in 1 mM NaCl. NaOH was added dropwise until the solution had reached a pH of approximately 11.5 for acid into base titrations. pH and conductivity were recorded automatically with HCl (0.1 M) as a function of acid volume added to the nanogel preparation (Mandel PC-Titrate, Mandel Scientific Company Inc., ON, Canada).

3.7 Transmission electron microscopy

A droplet of 4.5µL of the nanogel suspension at a concentration of 2mg/mL was dried on a copper TEM grid for 4 hours prior to imaging with a JEOL 1200EX TEMSCAN to observe nanogel morphology.

3.8 Modification of DMAEMA:DEGMA nanogels

Nanogels were prepared as described above with 45 mol% DMAEMA and 55 mol% DEGMA. Alterations of initiator and detergent concentrations were as described in Table 3.1.

Table 3.1 Modifications to composition of 45% DMAEMA formulations

Nanogel Formulation ID	Initiator (mol%)	CTAB (mM)
v50 5	0.5	0.92
v50 20	1.5	0.92
CTAB 35	1	0.96
CTAB 40	1	1.0

CTAB concentrations were explored between the critical micelle concentration of 0.92mM-10.mM and initiator concentrations were evaluated between 0.5-1.5mol%.

3.9 Synthesis of 2-hydroxyethyl disulfide diacrylate

Acryloyl chloride (Sigme-Aldrich) was added dropwise to a solution of triethylamine and dichloromethane. Reaction was carried at 0˚ C overnight in inert conditions and completion was observed through thin layer chromatography (TLC). Precipitate was removed through filtration and then rinsed sequentially with 1.0M $NaHSO_4$, 0.1M Na_2CO_3 and a brine solution. The organic phase was isolated and subsequently solvent was removed through rotovaporization at 50 rpm for 40 minutes at 20˚C. The product was purified through a column with a solvent system of 70% hexane: 30% ethyl acetate. Fractions were collected based on TLC and the solvent was removed through 3 hours of rotovaporization at 50 rpm 20˚C and final product was stored at 4˚C.

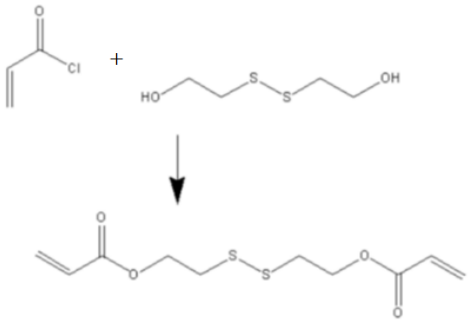

Figure 3.2 Crosslinker synthetic reaction

3.10 Confirmation of crosslinker structure with NMR

Samples were prepared by dissolving 10 mg in of diethyldisulfide diacrylate in deuterated dimethyl sulfoxide to confirm the structure, completion of the reaction and successful extraction of solvent. Solid-state H^1NMR was performed using Bruker AVANCE 200MHz NMR instrument. Data were analyzed on Topspin 3.5.

3.11 Degradation studies with TCEP and effect on size

Nanogel formulastions at a concentration of 3.68 mg/mL were incubated with 10 mM TCEP in milliQ water at room temperature for 40 days. DLS was performed to compare sizes between degraded particles and controls that were not incubated with TCEP under the same conditions. A Student's t-test used to determine whether changes in size were statistically significant.

3.12 Gel permeation chromatography (GPC) of degraded nanogel suspensions

To assess degradation profile of the nanogels, 1mg/mL of 45 mol% DMAEMA: 55 mol% DEGMA was degraded with various concentrations of TCEP and incubated at 37˚C for 40 days and filtered in the same method as described for HPLC prior to GPC. Gel permeation chromatography was performed in an aqueous solvent system of 0.5M Acetate 0.5M Sodium Acetate, pH 4.73, in a Waters GPC. Analysis was not performed for all formulations as they were not soluble in the solvent system (0.5M Acetate, 0.5M Sodium Acetate, pH 4.73). The solvent system was incubated with nanogel solutions (4.5mg/mL) tested at 37˚C for 2 days to observe miscibility. The 45% DMAEMA formulation was readily dissolved and therefore suitable for this test.

3.13 Turbidity assessment of degraded nanogel suspensions

Nanogels were degraded as described in chapter 3.10. Nanogels (3.68 mg/mL) both in the presence and absence of TCEP were plated (n=3) in a 96-Grenier well plate for absorbance reading at 500 nm using the Tecan M200 Infinite pro plate reader. Turbidity was calculated from the absorbance readings using the following equation, where A= absorbance.

$$Turbidity = e^{-2.303A}$$

3.14 Cloud point tests to determine lower critical solution temperature (LCST)

Nanogel suspensions were heated from 20°C to 80°C. Cloud point temperatures were determined as the onset of turbidity measured with the Cary 100 Bio UV-Visible spectrophotometer at a wavelength of 500 nm.

3.15 Titration with DLS and zeta potential monitoring

Samples were adjusted to pH 2.5 with 1 M hydrochloric acid. The nanogels were then titrated with 1mM KOH or 1M KOH up to pH 12 with both DLS and Zeta Measurements performed on the Zen3600 – Zetasizer Nano ZS and performed as described above with two measurements at each data point.

3.16 Purification of nanogels prior to cell tests and HPLC

Nanogels were filtered through HPLC grade Acrodisc 13mm nylon membrane syringe filters with a 0.2 μm pore size (Pall Corporation).

3.17 MTT Assay for metabolic effects of nanogels

Metabolic activity of 3T3 fibroblasts (10,000 cells/well) incubated with varying concentrations (1-1000μg/mL) of 45% DMAEMA were measured in 96-Greneir well plates in cell media (DMEM) with 10% fetal bovine serum. Samples were allowed to incubate for 48 hours at 37°C and 5% CO_2. Wells were washed and replaced with 100 μl phosphate buffered saline (PBS) and 10 μl MTT reagent (12mM 3-(4,5-dimethylthiazol-2-yl)-2,5-diphenyl terazolium bromide) stock) with control wells of PBS only, cell media only and MTT reagent. The plate was then incubated at 37°C and 5% CO_2 for 2 hours.

The supernatant was removed and 50 µl of dimethyl sulfoxide (DMSO) were added and mixed thoroughly with a pipette prior to a subsequent 10 minute incubation period at 37°C and 5% CO_2. The plate was read at 540nm with Tecan M200 Infinite pro plate reader.

3.18 Live/Dead cell for cytotoxicity analysis of nanogels

Cells were cultured and plated for nanogel live-dead test using identical conditions as outlined for the MTT assay for the same incubation time (48 hours). Cell media was removed and replaced with 50µL of PBS. A mixture of 2 µM calcein AM and 4 µM ethidiumin homodimer-2 (Et-d) in PBS (Sigma-Aldrich) was added to each test well and the control wells with cells only (nanogels absent). Live cell control wells were prepared with media and live stain or dead stain. Similarly, dead cell controls were prepared with both of the stains individually. The plate was incubated at room temperature in darkness for 30 minutes prior to imaging with a fluorescent microscope. Representative signals for live and dead cells were quantified using a fluorescent signal plate reader (Tecan M200 Infinite pro plate reader) with an excitation beam of 485nm / 530nm emmission (calcein) and 530nm excitation/645nm emission (Et-d) respectively.

3.19 Model drug loading and release

To load model drug, 3mg of dexamethasone phosphate was dissolved into 14 mg of DMAEMA nanogel formulations in 4-(2-hydroxyethyl)-1-piperazineethanesulfonic acid (HEPES) buffer for 60 hours in a shaking incubator at 37˚C. To remove drug that was not bound to the nanogel, ultrafiltration with Macrosep tubes with MWCO of 10kDa

at 10,000 g for 15 minutes was performed (Pall Corporation). The eluent was collected and analyzed after purification (as described above) by HPLC to quantify the amount of unbound drug. Negative controls were also prepared in the same manner but without drug loaded into the nanogel.

3.20 HPLC analysis of loaded drug and released drug

The drug loaded nanogels were transferred into 3.5kDa MWCO Spectra/Por® 6 cellulose dialysis tube membranes and placed in 10 mL falcon tubes to release into HEPES buffer in the absence/presence of tris(2-carboxyethyl)phosphine (TCEP – Cedarlane). The buffer was replaced at various time intervals maintaining sink conditions (<10% solubility of drug) throughout the release and collected for analysis. All samples were purified/filtered as described above in preparation for HPLC. Filtered samples were analyzed through a Phenomenex 5 μm (150mm x 4.60 mm) column at 1mL/min in an HPLC grade solvent system of 80:20 pH 7.4 PBS: acetonitrile.

3.21 -Determinations of loading capacity and loading efficiency of nanogels

Nanogel loading capacity (LC) was determined with the following equation

$$LC = \frac{A - B}{C} * 100$$

where A= total DXP (mg), B= unloaded “free” DXP (mg) and C= mass of nanogel formulation (mg).

Nanogel loading efficiency was similarily calculated as

$$L_{eff} = \frac{A - B}{A} * 100$$

3.22 Preparation of siRNA

1X siRNA resuspension buffer (Dharmacon) was prepared in RNAse free water according to manufacturer's instructions. siRNA was resuspended in the buffer to 10μM and stored at 4˚C prior to loading.

3.23 Sterilization of nanogels prior to transfection

Nanogels were transferred to a round bottom flask and lowered into an oil bath at 80˚C for 20 minutes. The mixture was allowed to cool at room temperature prior to DLS measurements of small sample sizes to ensure the integrity of the nanogels was not compromised through this process.

3.24 Loading of siRNA into nanogels

To load nanogels with gene therapeutic, 140 ng of siRNA was incubated with NG45 for 1 hour prior to the transfection study and rocked on a rotatory shaker at low speed. Loaded nanogels were spun for 2 minutes at 10,000 rpm in Nanosep (Pall Corporation) ultrafiltration tubes with 30 000 MWCO to separate loaded nanogels (NG-siRNA) from unbound siRNA. 2 μL of eluent was analyzed with Nanosight 2000c at 260 nm to determine the concentration of loaded siRNA by subtracting the amount within the eluent from the total amount loaded. The same amount of siRNA was used for all controls

outlined in the transfection protocol below. Nanogels loaded with siRNA were analyzed for size and charge using DLS and zeta potential analysis as per previous protocols outlined above. Encapsulation efficiency of loaded siRNA was calculated from the following equation.

$$EE = (m_{siRNA\ loaded} - m_{siRNA\ eluent}) \div m_{siRNA\ eluent} * 100$$

3.25 Transfection of siRNA into GFP-RPE cells

Human retinal epithelial (RPE) cells were transduced Cignal Lenti Reporter lentivirus with green fluorescence protein (GFP) from Qiagen as per company instructions. A 96-well Grenier plate was seeded to 70% confluency with RPE cells and allowed to adhere to the plate in Opti-Mem with 1% fetal bovine serum (Life Technologies) for 24 hours prior to addition of nanogel formulations and controls. Transfection was monitored by fluorescence microscopy to observe a decrease in GFP fluorescence and scanned with the TECAN M200 Infinite pro plate reader at 475 nm excitation and 509 nm emission was taken throughout transfection period of 68 hours. All tests were run in quintuplicates to observe differences in fluorescence. Controls included RPE cells only, nanogels (45% formulation) only, nanogels/negative siRNA, nanogels/GFP-siRNA, GFP-siRNA and GFP-siRNA/Dharmafect (Dharmacon).

Chapter 4. RESULTS & DISCUSSION

4.1 Development of cationic nanogel synthesis

Nanogel size and charge were used to screen potential materials for their applicability in gene delivery applications. The results shown Figure 4.1.1 display the

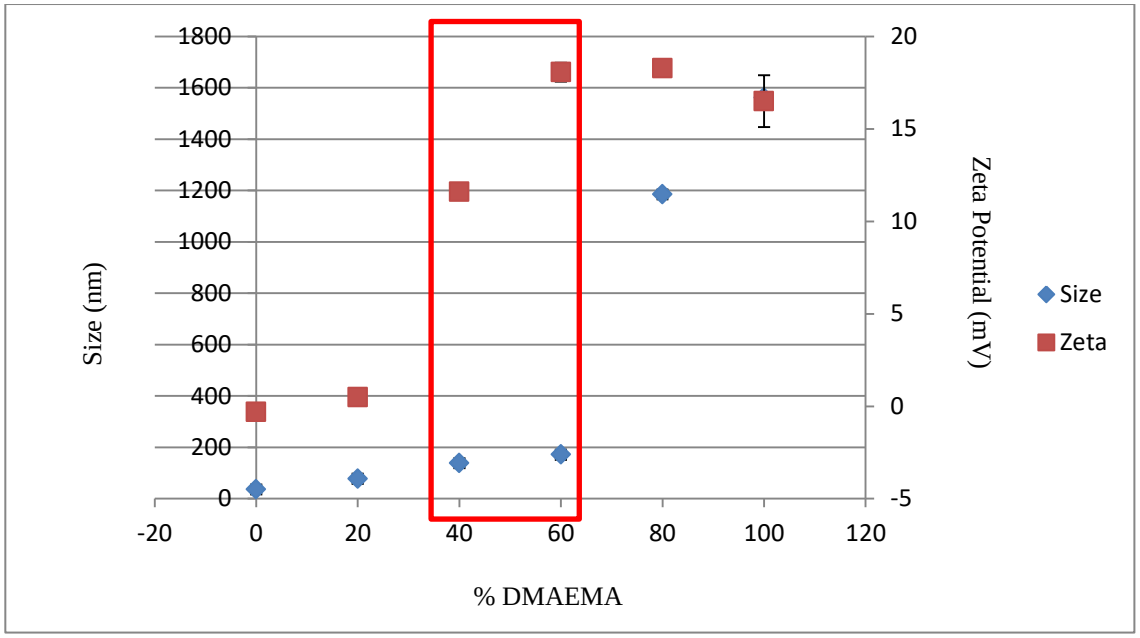

Figure 4.1.1 Effect on size and zeta potential with increasing DMAEMA content in nanogel formulations. *Error bars were calculated as the standard deviation of five measurements. Hilighted area refers to formulae with both ideal size and charge. (Zeta potential > 10mV = positive charge) Nanogels refered to as NG"%DMAEMA". Ie. 0% DMAEMA = NG0*

various sizes and charges of the nanogel formulations synthesized. This array was analyzed to establish a synthetic method to produce cationic nanogels that were small enough to undergo endocytosis. Sizes between 50nm – 200nm are appropriate for these purposes, as they do not elicit immune responses and promote encapsulation (Yin Win & Feng, 2005). Nanoparticles with sizes less than 200 nm were only formed when 60%

DMAEMA or less was used. A zeta potential greater than 10 mV signified a cationic particle. It can therefore be seen that batches with 40-100% DMAEMA were positively charged. The trends also showed that increasing DMAEMA content increased positive character which is due to the presence of the protonated amine group which has a pKa of 8.9 resulting in positively charged particles at physiolgical pH.

Endocytosis is not only promoted by electrostatic interactions between a cationic nanogel and the negative cellular surface; morphology also plays a role. It has been shown that spherical nanoparticles readily undergo endocytosis (Chithrani & Chan, 2007). TEM images shown in Figure 4.1.2 provide insight into the nanogel morphology and the size distribution of the nanogel formulations prepared.

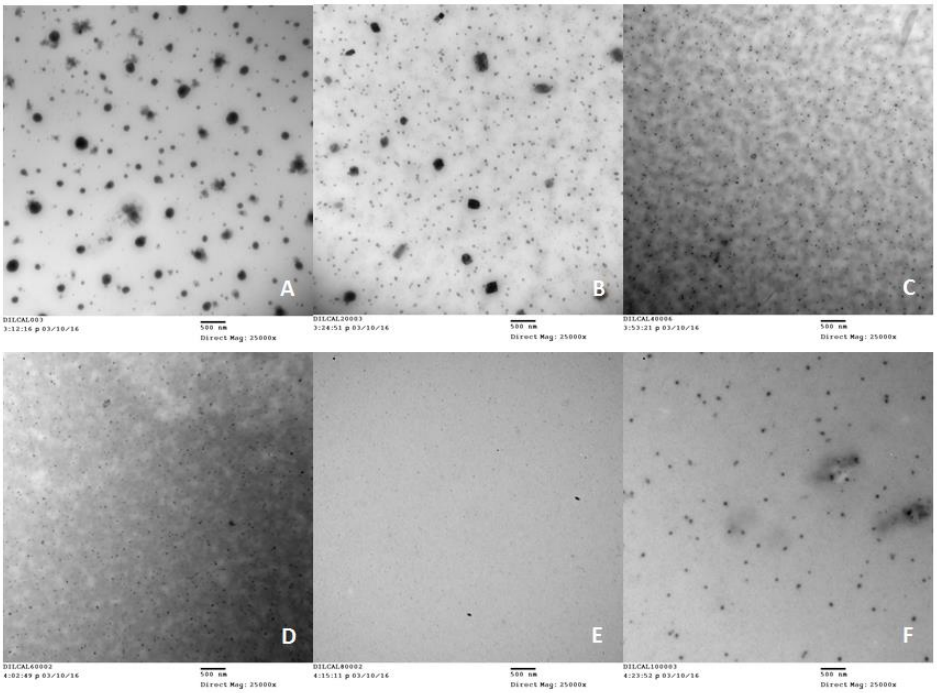

Figure 4.1.2 Nanogel imaged by transmission electron microscopy. *Images of nanogel formulations were all taken at 25000X magnification with all size bars set to 500nm.(A:NG0, B:NG20, C:NG40, D:NG60, E: NG80, F:NG 100)*

The nanoparticles appeared spherical and, within the 40-60% DMAEMA content range, showed higher monodispersity (Figure 4.1.2).This is also reflected in lower polydispersity indices as seen in Table 4.1.1. NG0 and NG20 appeared in TEM to have high polydispersity contrary to the measured values shown in Table 4.1.1, although this could be due to the drying process that the samples must undergo for TEM analysis.

Table 4.1.1 Nanogel Formulation Characteristics
DMAEMA content determined by titration, polydispersity index from DLS measurements, concentration of nanogels through gravimetric analysis and Nanosight and transmittance data.

Nanogel ID	NG0	NG20	NG40	NG35	NG40	NG45	NG50	NG60	NG80	NG100
DMAEMA (%) Theoretical	0	20	30	35	40	45	50	60	80	100
DMAEMA (%)*	0	4.47	--	--	9.48	--	--	14.95	18.99	25.56
Polydispersity index**	0.18	0.15	0.07	0.16	0.16	0.18	0.25	0.32	0.36	0.27
Particle *** Concentration (particles/mL)	8.96 E8	4.43E8	--	--	2.03 E8	1.07 E9	--	4.01 E8	2.51E8	6.72E8
Concentration (mg/mL)****	19.64	13.02	11.97	10.93	8.19	9.65	8.47	6.35	4.77	3.68
Transparency (% Transmittance)*****	0.89	64.49	--	--	93.77	--	--	98.17	98.99	100.01

* Potentiometric-conductometric titrations were performed as outlined in Chapter 3 to determine actual DMAEMA content. ** PDI was measured during DLS measurements of size.*** Determined through Nanosight **** Determined through gravimetric analysis *****Calculated from absorbance readings. All methods outlined in Chapter 3.

DEGMA is a thermosensitive polymer that undergoes phase separation; therefore it is possible that what is observed in the images is a drying artefact during drying at room temperature prior to TEM imaging (Figure 4.1.2). Sizes can be seen to increase

dramatically with the addition of larger amounts of DMAEMA. These nanogels would be highly water-swelling due to high charge distribution attributed to the protonated amine group. Therefore it is not unexpected to see an increase not only in the positive charge with DMAEMA incorporation, but also the size.

High polydispersity was observed in NG100, which would be indicative of a varying size population. It is plausible that the entire DMAEMA population was not protonated at pH 4.5 during synthesis, leading to to a non-uniform distribution of charge, thus destabilizing micelle formation which is directly indicative of nanogel size (Makino, Hara, Hara, Ozeki, & Kimura, 2014). Further exploration of this phenomenon was not pursued as these particles were too large to undergo endocytosis (Yin Win & Feng, 2005). Due to these factors, the observation of highly polydisperse nanogel populations is not unexpected.

The overall purpose of the array of nanogel formulations was to establish a data set that would lead to the the development of a cationic nanogel. Batches NG40 and NG60 not only show promise in size, charge and morphology, but due to the high transmittance observed in Table 4.1.1 show promise as potential nanocarriers for ophthalmic applications. Based on these results, formulations with compositions between these two ranges were further evaluated. Formulations comprised of 35%-55% DMAEMA were synthesized to explore potential candidates for an optimal formulation for future *in vitro* studies. The size and zeta potential data in Figure 4.1.3 followed the

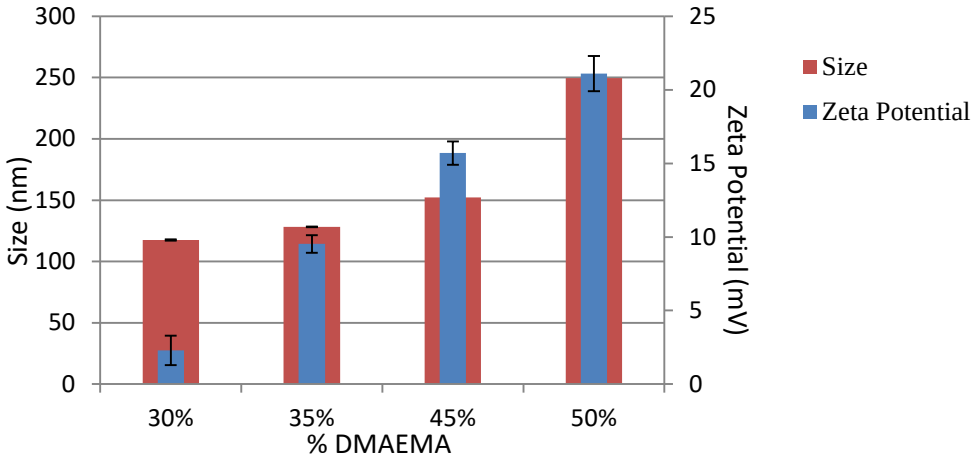

Figure 4.1.3 Additional nanogel compositions to determine ideal formulation by zeta potential and size. *Error bars were calculated as the standard deviation between five measurements. Size was determined by DLS and a positive charge determined through zeta potential > 10mV.*

same trends as with Figure 4.1.1, with size and zeta potential both increasing with increasing DMAEMA content, as expected.

From Figure 4.1.3, the 45% DMAEMA formulation (NG45) was considered for further study due to its positive charge and size (152 nm), which fulfilled both requirements as a nano-sized and positive nanogel. Additionally, the TEM image (Figure 4.1.4) shows a monodisperse formulation, thereby validating NG45's potential.

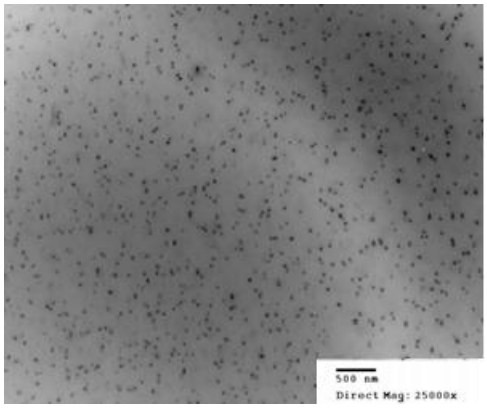

Figure 4.1.4 TEM image of NG45 at 25000X with size bar set to 500nm.

The high transmittance of light (Table 4.1.1) and the transparency of the nanogels at room temperature shown in Figure 4.1.5, suggest that these nanogels not only have characteristics suitable for cell entry but have physical properties that demonstrate usefulness as an ophthalmic nanocarrier.

Figure 4.1.5 Images of nanogel formulations with varying contents of DMAEMA (remainder being DEGMA). *From left to right: 0,20,30,35,40,45,50,60,80,100 (%DMAEMA). Images were taken of aliquots at room temperature after brief agitation.*

Further optimization of NG45 was briefly explored using various detergent and initiator concentrations. The original recipe used a detergent concentration within the critical micelle concentration (CMC) of 0.92 mM-1.0 mM. As the original recipe was made with 0.92mM CTAB, higher concentrations were investigated to observe the effect on size. According to literature, increasing concentrations of detergent lead to the formation of smaller micelles for precipitation polymerization, resulting in smaller nanoparticles (Gao *et al*., 2004). In Figure 4.1.6, this phenomenon was observed as CTAB40 did in fact have a smaller size than was reported for CTAB35.

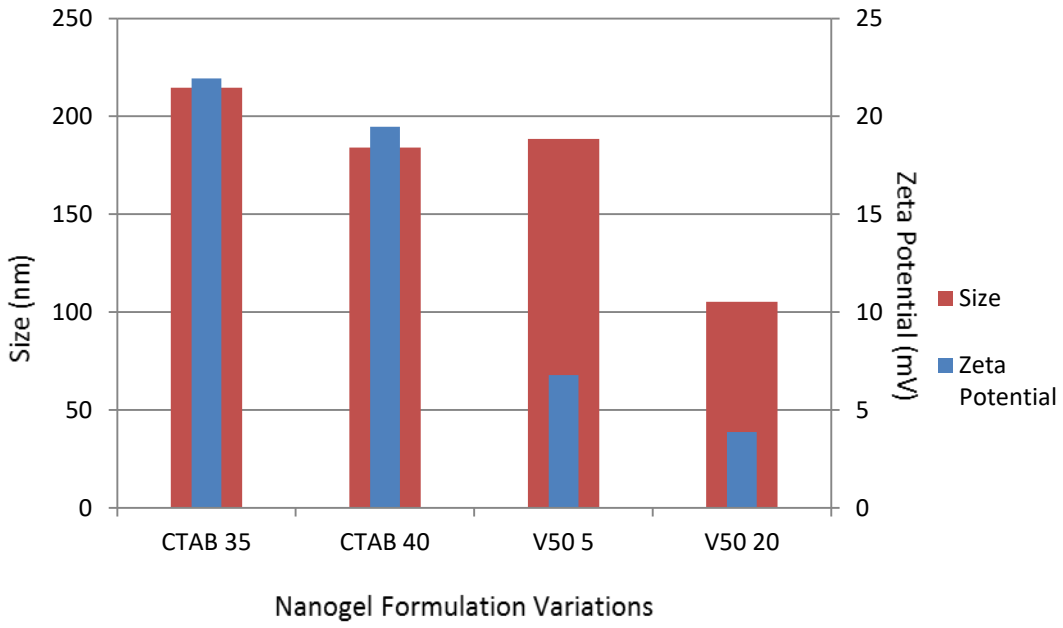

Figure 4.1.6 Effect on size and zeta potential of modifications of NG45 with initiator (v50) and detergent (CTAB). *DLS determined size and zeta potential >10mV indicated positive charge. Formulae compositions can be found in Table 3.1.*

However, these formulations demonstrated an inverse effect than NG45, which used the lowest CMC. Dispersion and precipitation polymerization were both achievable by the set reaction conditions but at low detergent concentrations it appears that dispersion was favoured over precipitation. Often dispersion and precipitation polymerization are used interchangeably in literature and a defining difference has not been reported. Instead, nanogel characteristics such as monodispersity, and the formation of spherical and nano-sized particles have been shown to indicate dispersion polymerization (Sanson & Rieger, 2010). Therefore, since NG45 gave highly spherical and monodisperse nanoparticles, it is likely that the dispersion polymerization mechanism instead of precipitation occurred in this case. Since the original recipe resulted in favourable sizes, appropriate for endocytosis, original conditions were maintained.

The effect of initiator concentration was also observed; the results are shown in Figure 4.1.6. It showed that decreasing concentration of thermal initiator, v50, led to decreased size and zeta potential. It is not unexpected that increasing initiator amounts (v20) would give rise to smaller particles and less DMAEMA incorporation as similar trends have been observed in the literature (Liu, Wang, Zhang, & Zhang, 2016). Through this study, a cationic nanogel was successfully synthesized and characterized. The particles prepared show characteristics which suggest that they may be promising for gene delivery in ophthalmic applications.

4.2 Degradability potential of nanogels

DEGMA and DMAEMA were used to synthesize nanogels crosslinked with a synthetic crosslinker that contained a disulphide bridge. The purpose of synthesizing a crosslinker with this bond, was to allow for degradation in vivo via the disulphide bridge due to the presence of a 20 μM intracellular concentration of glutathione (Meng, Hennink, & Zhong, 2009). Not only does glutathione reduce these bonds, but the reducing intracellular environment also promotes hydrolytic cleavage. Therefore, nanopreparations containing this a disulphide containing crosslinker have significant potential for intracellular degradation. Figure 4.2.1 provides confirmation of the chemical structure of 2-hydroxy disulphide diacrylate.

Figure 4.2.1 Crosslinker synthesis confirmation through H[1]NMR. *Superimposed image of 2- hydroxyl disulphide diacrylate with H[1]NMR shift predictions estimated by ChemDraw Ultra 8.0.*

The chloroform solvent peak was at 7.24 ppm; all other protons were represented by peaks in the NMR spectrum. To assess the potential degradation capabilities of the particles, NG20/40/60 were incubated under reducing conditions. Subsequently, DLS was performed to observe a decrease in size, with the results shown in Figure 4.2.2.

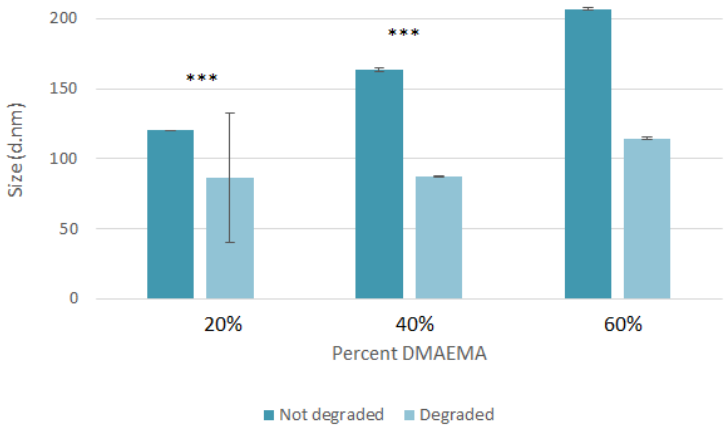

Figure 4.2.2 Effect of reducing environment on nanogel size verified by DLS. *Nanogels were incubated at room temperature for 40 day incubation period with or without 10mM TCEP (reducing agent). Error bars were calculated from standard deviation of five measurements. Student t-tests were run with a p-value of 0.001 to determine significant differences.*

As can be seen, all formulations showed a decrease in size upon incubation with the reducing agent TCEP. Formulations NG20 and NG40 showed a statistically significant shrink, which supports a theory of degradation. Combined with the GPC results for of NG45 shown in Figure 4.2.3 where the polymer peak at 25 minutes was

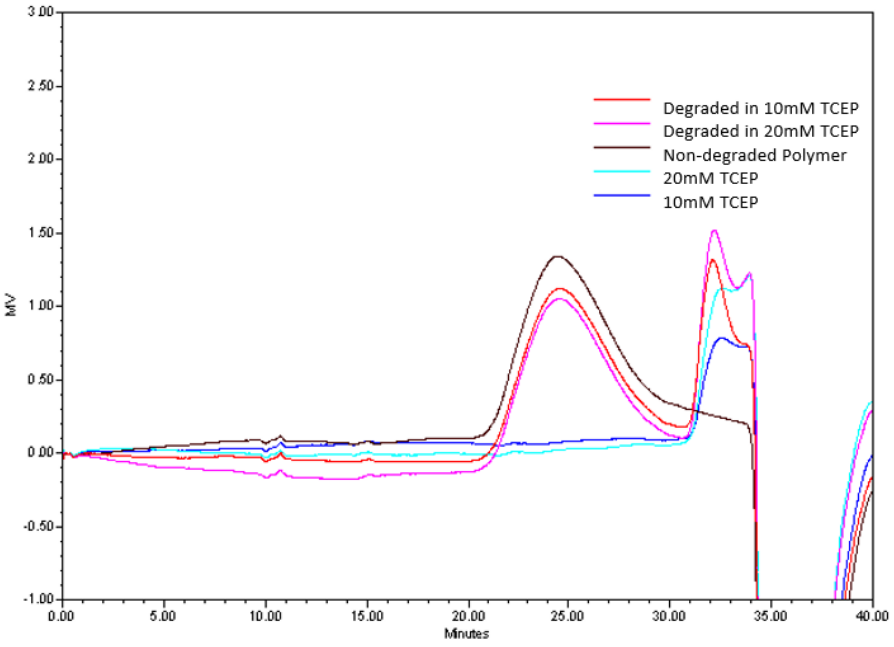

Figure 4.2.3 GPC of NG45 in various reducing environments. *Nanogels were incubated at 37˚C during 10 day incubation period.*

decreased, it can be predicted that these nanogels have the potential to undergo degradation in the cellular environment. These results are further supported by the turbidity measurements shown in Figure 4.2.3. Turbidity, a measurement of light scattering, when measuring a suspension of particles (Scherer, Leung, Owyang, & Shire, 2012). Therefore, it is evident from the decrease in size and the drastic decrease in turbidity of control samples and nanogels in the presence of TCEP, that the nanogels undergo a significant response in reducing environments. It is predicted that this response

is credited to the presence of disulphide crosslinker that will reduce to free thiol groups when undergoing a reduction reaction with any reducing agent (Meng *et al*., 2009). Taken together with the decrease in amount of polymer found in GPC, there is significant support for predicted intracellular degradation.

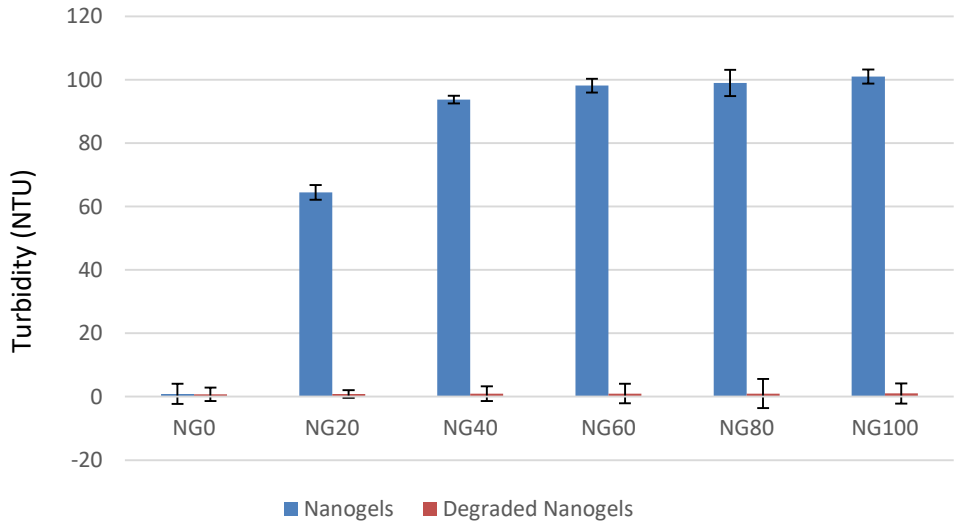

Figure 4.2.4 Impact of reducing nanogels by turbidity measurements. *Turbidity was calculated using absorbance measurements as described in section Error bars were calculated from three repeat measurements.(n=3)*

4.3 Potential for NG45 in biological applications

The risk of using a cationic polymer to create nanogels is that the amine group is known to be cytotoxic (R7). To evaluate the effect of increasing DMAEMA content which was shown earlier to increase the positive charge on the nanogel (Figure 4.1.1.), *in vitro* studies were performed. Both a live-dead assay in 3T3 fibroblasts and a

mitochondrial activity assessment through an MTT assay were analyzed to observe the biological impact of incubation with the nanogel formulations.

Figure 4.3.1 displays 3T3 fibroblasts incubated with high 100µg/mL of NG40 and NG60. Compared to the control cells, incubation with the nanogels for 72 hours had minimal impact on cell death. The results suggest that incubation with NG60 resulted in slightly more cell death than was observed in NG40, which can be attributed to the increase in amine content from the DMAEMA.

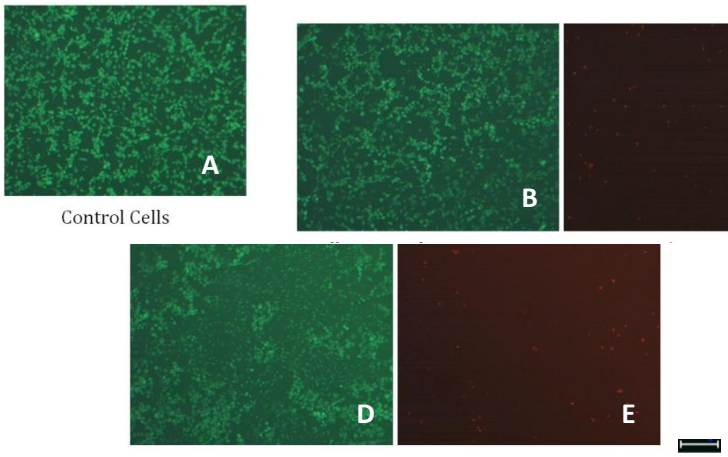

Figure 4.3.1 Live-dead test in 3T3 fibroblasts. *A: Control cells seeded at equal density to test wells.NG40 applied to cells at 100micrograms/mL, live cells (B), dead cells (C) NG60 incubated with cells at 100 micrograms/mL, live cells (D), dead cells (E). Scale bar = 100µm.*

The MTT results, shown in Figure 4.3.2 also showed that with increasing DMAEMA, there was a lower level of viability. Similarly, the results suggest that high concentrations of nanogels may also lead to decreased cell compatibility. The NG45

nanogels were found to have minimal impact on cell proliferation at low concentrations. Transfection studies at a concentration of 20 µg/mL of NG45 would therefore not be expected to negatively impact cell viability.

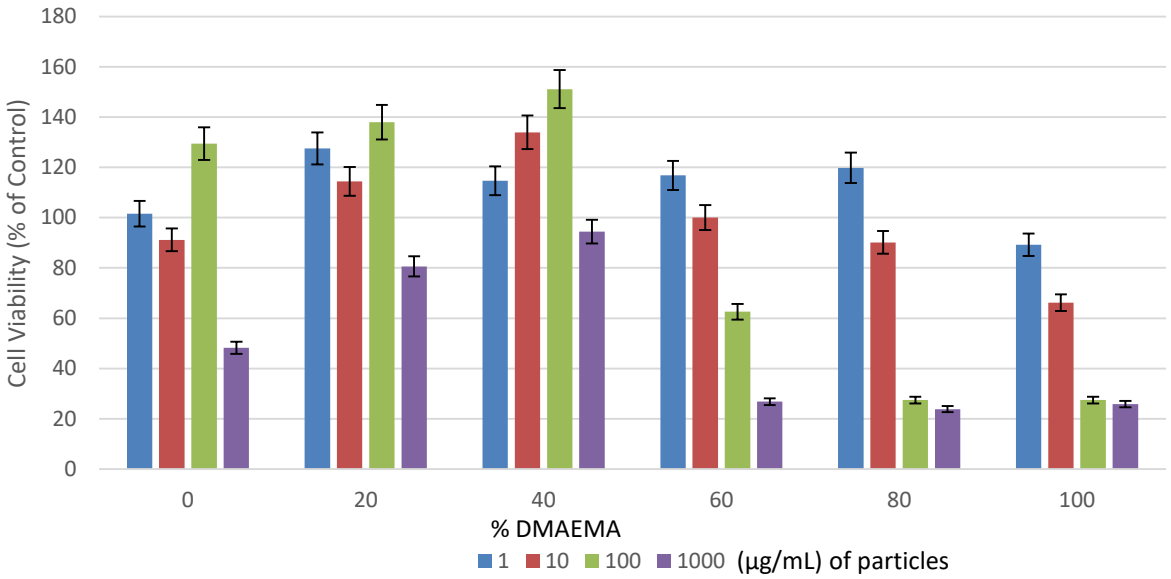

Figure 4.3.2 Cytotoxicity assessment of various nanogel formulations incubated in 3T3 fibroblasts at 1-1000micrograms/mL. *Error was calculated from the standard deviation of five measurements.*

4.4 Impact of using "smart materials"

Smart materials are often used in drug release vehicles to allow for stimuli responsive release of therapeutics. To investigate the impact of using thermosensitive DEGMA and pH-sensitive DMAEMA various studies were performed. To observe the lower critical solution temperature that is characteristic of DEGMA, all formulations were monitored for their LCST based on the onset of turbidity as measured using absorbance

(Figure 4.4.1). It can be seen that a higher DEGMA content in the nanogels resulted in an LCST

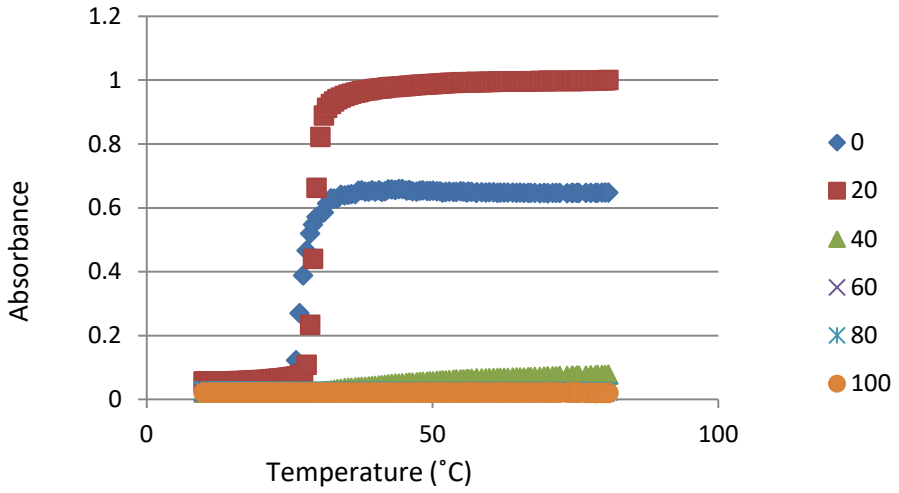

Figure 4.4.1 Lower critical solution temperature as determined through UV reading at 500nm. *The point of turbidity indicates an LCST.*

that occurred at 29˚C. This observation was only seen in NG0 and NG20 which is expected due to their high thermosensitive polymer content. To observe the effect of the thermosensitivity of DEGMA on the NG45 formulation, particle size was monitored by DLS. From the results shown in Figure 4.4.2, it is evident that this property lies only with DEGMA and that the NG45 formulation exhibits minimal thermosensitive properties. In a similar study, pH-sensitivity was analyzed by monitoring both the size and charge of nanogels undergoing base into acid titration (Figure 4.3.3). NG0 and NG100 showed very NG0. Figure 4.4.3 shows that the size and charge remained relatively the same during titration when the pH-sensitive monomer, DMAEMA was absent.

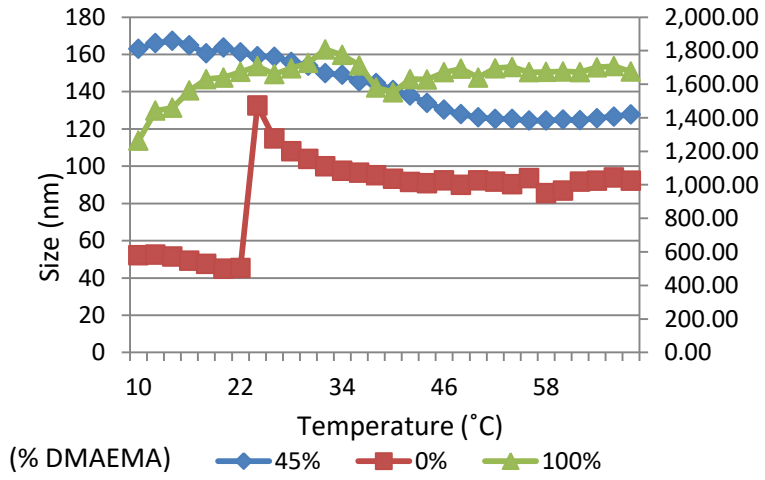

Figure 4.4.2 Size determination of various nanogel formuations with DLS in response to temperature. *0% DMAEMA formulation was plotted on the secondary axis to be able to compare the three formulae despite its large size.*

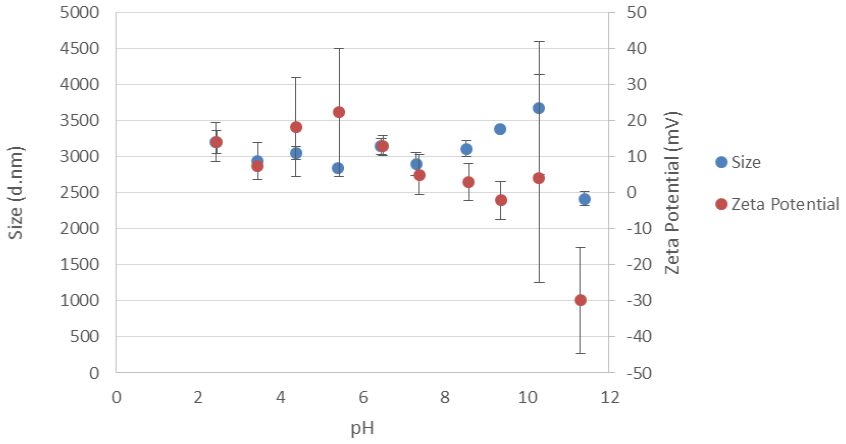

Figure 4.4.3 Size and charge monitored by DLS and zeta potential respectively during a base into acid titration of NG0. *Error was determined through standard deviation between two measurements.*

different sensitivities to pH as expected due to the lack of a pH-sensitive characteristic in Contrarily, Figure 4.4.4 shows that size and charge were affected with increasing pH for NG100. As conditions get increasingly basic, deprotonation of the amine group occurred which explains the decrease in zeta potential during titration. The size also decreases which can be attributed to deswelling of the nanogels due to lack of repelling positive charge units present in DMAEMA.

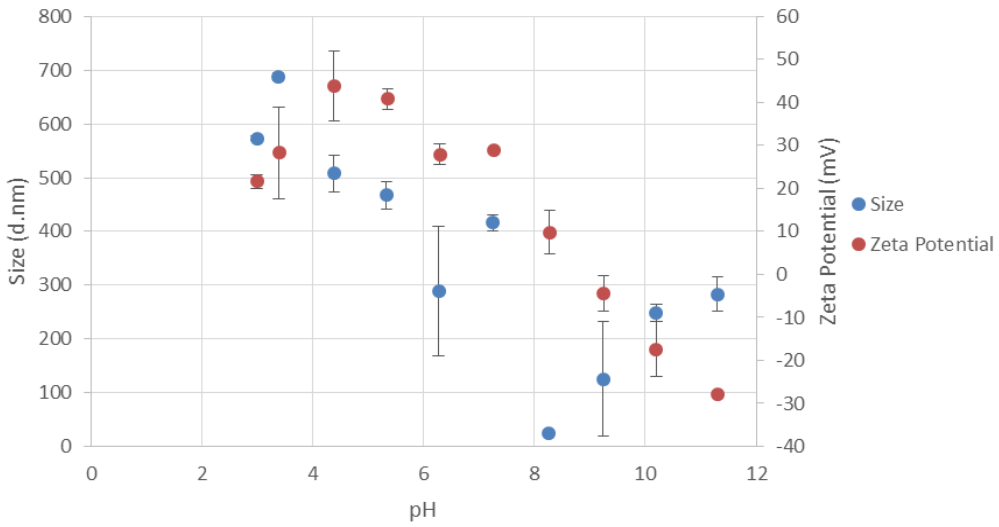

Figure 4.4.4 Size and charge monitored by DLS and zeta potential respectively during a base into acid titration with NG100. *N=2, error was determined from standard deviation between measurements.*

Figure 4.4.5 shows the response of the NG45 formulation to various pH environments. It appears that the nanogel can increase and decrease in size, depending on the pH of the system. The largest swelling capacity conveniently occurs at approximately physiological pH, which can be used to facilitate endosomal escape after cell entry. This swelling capacity could also be examined for enhancing loading capacity by adding drug

when swollen and injecting nanogel when collapsed. This study elucidates the pH-sensitive nature of NG45 which can be further explored to enhance this nanocarrier as a stimuli-responsive vehicle.

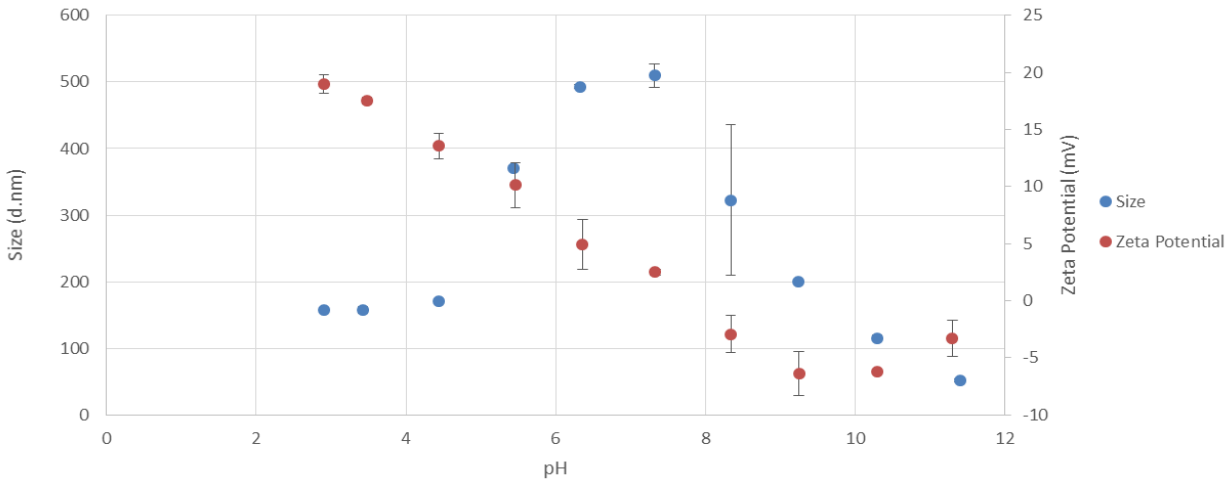

Figure 4.4.5 Size and zeta potential monitored by DLS and zeta potential using NG45.*Error determined from standard deviation of n=2. Measurements of size and charge were enabled through base into acid titration.*

These results altogether show the great potential for NG45 as a delivery vehicle, but it is important to note that while this vehicle is stable at physiological pH, Figure 4.4.6 shows that in extreme conditions the spherical nature is lost and aggregation can occur. Therefore future studies, even when using swelling abilities by altering various pH, should keep in mind the nanogel stability.

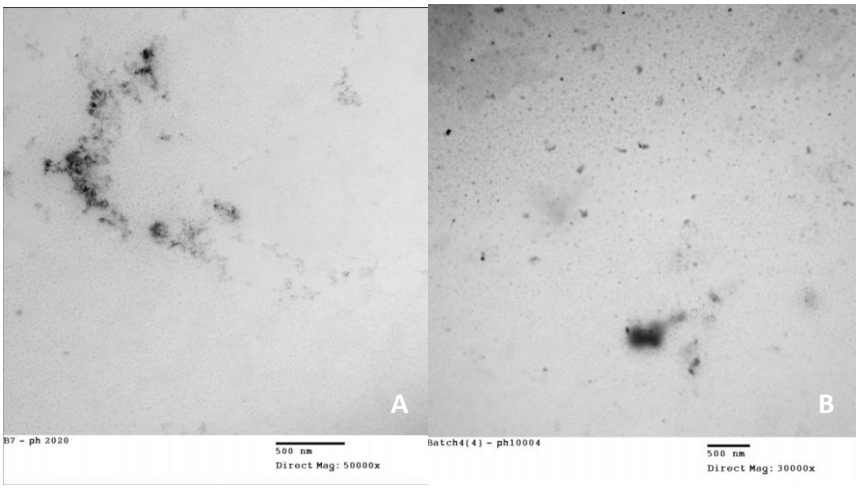

Figure 4.4.6 Effect of pH on NG45. *Incubation at pH 2 (A) and pH10 (B). Size bars = 500nm. Images taken at 50000X with TEM.*

4.5 Nanogels as delivery vehicles.

The properties described above suggest that these nanogels may have utility for the delivery of genetic material as well as the delivery of drugs. Table 4.5.1 describes the loading capacity (LC) and efficiency (LE) observed with different nanogel formulations. All vehicles had a high LC and LE, but the highest capacity and efficiency was found with NG45 optimized nanogel formula.

Table 4.5.1 Loading capacity and efficiency of nanogel formulations with model drug dexamethasone phosphate.

	NG0(%)	NG45(%)	NG100(%)
LC	330.67	385.33	342.67
LE	82.67	96.33	85.67

Figure 4.5.1 displays the release of model drug dexamethasone phosphate, DXP, a negatively charged, hydrophilic drug, in physiological buffer, HEPES. This drug was chosen for its negative charge as a surrogate prior to siRNA delivery.

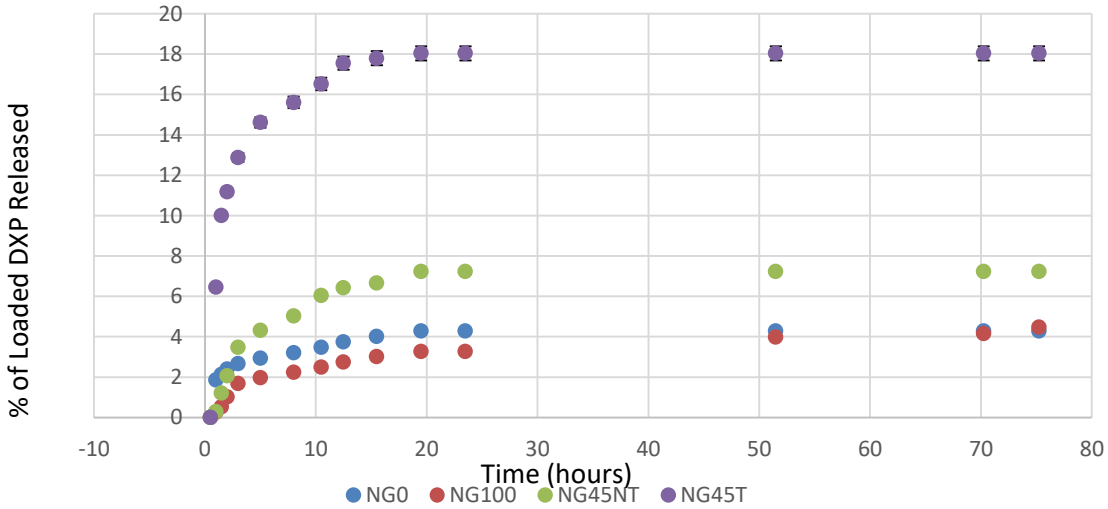

Figure 4.5.1 Model drug release of DXP. *NG45 loaded with DXP released; NG45T: in the presence of TCEP, NG45NT: in the absence of TCEP. Error from standard deviation of n=2.*

Simultaneously, the effect of a reducing intracellular environment using the reducing agent TCEP on release properties was evaluated using the NG45 formula. Figure 4.5.1 shows that NG0, NG100 and NG45 all showed rapid release of the drug, within 24 hours. Since NG45 had a higher loading capacity, a greater quantity of DXP was released when NG45 used and the drug was released into a reducing medium. 6% of drug was released overall when not in the presence of TCEP, but there was an 11% increase in DXP unloading in the reducing environment. This also provides evidence for the degradation of the disulphide bridge found in the synthetic crosslinker. For the

purpose of siRNA delivery, this is advantageous, as the therapeutic will be more readily released in a reducing environment. Since the cell has a highly reducing environment compared to the more oxidizing extracellular atmosphere, it is likely that the target drug/gene therapeutic will be released intra rather than extracellularly. siRNA does not require high doses for efficacy but it is an expensive alternative to other drug therapies. NG45 would promote the potential for siRNA delivery not only for properties favouring cell entry but due to preferential intracellular unloading.

In a preliminary study to test the application of NG45 as a siRNA nanocarrier, a transfection was employed in series with an industry standard transfection reagent (DF:Dharmafect). From the studies performed in human retinal epithelial cells transduced with green fluorescence protein (GFP-RPE), siRNA delivery should decrease the overall fluorescence to indicate gene silencing. Since the positive control utilizing Dharmafect complexed with siRNA did not exhibit a noticeable silencing effect, optimization must be oerformed. Areas that can be explored further are siRNA concentration, cell confluency levels, and cellular media composition to encourage gene silencing. Incubation with NG45 at 20µg/mL did not appear to have an effect on the RPE cell line (Figure 4.5.2).

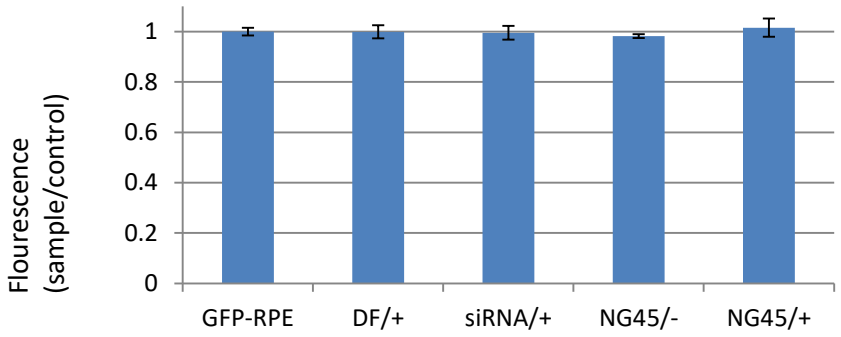

Figure 4.5.2 Transfection study measuring the fluorescence of GFP-RPE cells. ***GFP****-RPE:Control well with cells only, DF/+:Dharmafect transfection reagent complexed with GFP-targetting siRNA, siRNA/+: GFP-targetting siRNA, NG45/-: NG45 complexed with non-targetting siRNA, NG45/+: NG45 complexed with GFP targetting siRNA. Error bars derived from standard deviation of ten repeat measurements.*

Therefore, future work will be directed into optimization of transfection conditions. Further investigation would benefit future transfection studies, but taken together with the sufficient release of DXP in reducing environments and the non-cytotoxic levels of applicable doses of NG45, there is potential to pursue this line of research for local siRNA delivery.

Chapter 5. CONCLUSIONS

A variety of novel nanogel formulations were prepared using DEGMA and DMAEMA in ratios ranging between 0 and 100%. The nanogels were characterized using a variety of techniques. It was found that a positively charged vehicle of appropriate size with potential for endocytotic delivery was created using a DMAEMA content of 45%. Nanogels with DMAEMA contents of less than 45% exhibited less positive charge while nanogels prepared with the DMAEMA contents of greater than 45% were highly swollen; particles prepared at this concentration had sizes greater than acceptable sizes for endocytosis. Through this process an ideal formulation "NG45" was established that had spherical morphology with a monodisperse size population.

The array of nanogels synthesized helped to establish NG45 and served as a comparison to assess physical and chemical properties. Using these formulations it was determined that NG45 was not a thermosensitive nanogel but in fact had pH-sensitivity due to the content of DMAEMA.The cytotoxicity of the nanogels was assessed using 3T3 fibroblasts. The MTT and live-dead assays taken together demonstrated that these particles show good biocompatibility. Release of dexamethasone phosphate from the particles demonstrated the potential of the nanogels for the delivery of drugs. While the release was relatively rapid, the results demonstrate the potential of the nanogels for the delivery of siRNA to cells.

Due to the high loading efficiency of negatively charged DXP NG45, it showed particular promise as a gene therapeutic carrier. Unfortunately, silencing was not observed even in positive controls so there is no data supporting or rejecting this

particular application. Future studies will focus on transfection studies, exploring potential inhibitors to the silencing process. Various cell densities can also be plated and incubated at different times with the silencing agent to observe the effects. However additional troubleshooting is required to improve the siRNA efficiency itself and not the transfection reagent that was developed.

Future work would benefit from utilizing the pH-sensitive property of the nanogels to control release properties. Injecting these nanogels at a slightly acidic/basic pH where they are in a collapsed state could potentially reduce the initial burst release. However, for the application of siRNA, the need for delivery to the intracellular environment prior to extracellular degradation will be necessary. Delivery to the cell provides a greater challenge than the prolonged effect of the therapeutic. Studies should also be performed using the NG45 formulation in harsher reducing conditions and a variety of physiological buffer systems to mimic the intravitreal environment.

Ultimately, transfection studies should be optimized to observe the silencing efficiency compared to market standards. Analysis of the cellular uptake of this nanovehicle must be performed to assess the enhancement of endocytosis due to charge and size. This evaluation would also benefit interpretation of silencing effects in transfection experiments to elucidate if the nanogel in fact delivered siRNA intracellularly to produce a silencing effect and to validate the necessity for the nanogel carrier.

Chapter 6. REFERENCES

Acemoglu, M. (2004). Chemistry of polymer biodegradation and implications on parenteral drug delivery. *International Journal of Pharmaceutics*, *277*(1-2), 133–9.

Agashe, H. B., Dutta, T., Garg, M., & Jain, N. K. (2006). Investigations on the toxicological profile of functionalized fifth-generation poly (propylene imine) dendrimer. *The Journal of Pharmacy and Pharmacology*, *58*(11), 1491–8.

Alexandru, M. R., & Alexandra, N. M. (2016). Wet age related macular degeneration management and follow-up. *Romanian Journal of Ophthalmology*, *60*(1), 9–13.

Ayame, H., Morimoto, N., & Akiyoshi, K. (2008). Self-assembled cationic nanogels for intracellular protein delivery. *Bioconjugate Chemistry*, *19*(4), 882–90.

Azevedo, H., & Reis, R. (2004). Understanding the Enzymatic Degradation of Biodegradable Polymers and Strategies to Control Their Degradation Rate. In *Biodegradable Systems in Tissue Engineering and Regenerative Medicine*. CRC Press.

Boussif, O., Lezoualc'h, F., Zanta, M. A., Mergny, M. D., Scherman, D., Demeneix, B., & Behr, J. P. (1995). A versatile vector for gene and oligonucleotide transfer into cells in culture and in vivo: polyethylenimine. *Proceedings of the National Academy of Sciences of the United States of America*, *92*(16), 7297–301.

Bressler, S. B. (2009). Introduction: Understanding the Role of Angiogenesis and Antiangiogenic Agents in Age-Related Macular Degeneration. *Ophthalmology*,

116(10), S1–S7.

Bucolo, C., Drago, F., & Salomone, S. (2012). Ocular drug delivery: a clue from nanotechnology. *Frontiers in Pharmacology*, *3*, 188.

Check, E. (2005). News Feature: A crucial test. *Nature Medicine*, *11*(3), 243–244.

Chithrani, B. D., & Chan, W. C. W. (2007). Elucidating the mechanism of cellular uptake and removal of protein-coated gold nanoparticles of different sizes and shapes. *Nano Letters*, *7*(6), 1542–50.

Del Amo, E., & Urtti, A. (2008). Current and future ophthalmic drug delivery systemsA shift to the posterior segment. *Drug Discovery Today*, *13*(3-4), 135–143.

DelMonte, D. W., & Kim, T. (2011). Anatomy and physiology of the cornea. *Journal of Cataract & Refractive Surgery*, *37*(3), 588–598.

Deng, Y., Wang, C. C., Choy, K. W., Du, Q., Chen, J., Wang, Q., … Tang, T. (2014). Therapeutic potentials of gene silencing by RNA interference: principles, challenges, and new strategies. *Gene*, *538*(2), 217–27.

Deshayes, S., & Kasko, A. M. (2013). Polymeric biomaterials with engineered degradation. *Journal of Polymer Science Part A: Polymer Chemistry*, *51*(17), 3531–3566.

Dorwal, D. (2012). Nanogels as novel and versatile pharmaceuticals. *International Journal of Pharmacy and Pharmaceutical Sciences*, *4*(3), 67–74.

Duvvuri, S., Majumdar, S., & Mitra, A. K. (2003). Drug delivery to the retina: challenges and opportunities. *Expert Opinion on Biological Therapy*, *3*(1), 45–56.

Edelhauser, H. F., Rowe-Rendleman, C. L., Robinson, M. R., Dawson, D. G., Chader, G. J., Grossniklaus, H. E., … Wong, W. T. (2010). Ophthalmic Drug Delivery Systems for the Treatment of Retinal Diseases: Basic Research to Clinical Applications. *Investigative Opthalmology & Visual Science*, *51*(11), 5403.

Fulmer, T. (2009). Breaching the retinal barrier. *Science-Business eXchange*, *2*(42).

Funke, W., Okay, O., & Joos-Müller, B. (n.d.). Microgels-Intramolecularly Crossünked Macromolecules with a Globular Structure. In *Microencapsulation Microgels Iniferters* (pp. 139–234). Berlin, Heidelberg: Springer Berlin Heidelberg.

Gao, H., Zhu, R., Yang, X., Mao, S., Zhao, S., Yu, J., & Du, Y. (2004). Properties of polyethylene glycol (23) lauryl ether with cetyltrimethylammonium bromide in mixed aqueous solutions studied by self-diffusion coefficient NMR. *Journal of Colloid and Interface Science*, *273*(2), 626–31.

Geroski, D. H., & Edelhauser, H. F. (2000). Drug delivery for posterior segment eye disease. *Investigative Ophthalmology & Visual Science*, *41*(5), 961–4.

Guymer, R., Luthert, P., & Bird, A. (1999). Changes in Bruch's membrane and related structures with age. *Progress in Retinal and Eye Research*, *18*(1), 59–90.

Guzman-Aranguez, A., Loma, P., & Pintor, J. (2013). Small-interfering RNAs (siRNAs) as a promising tool for ocular therapy. *British Journal of Pharmacology*, *170*(4),

730–747.

HÃbel, S., Koburger, I., John, M., Czubayko, F., Hadwiger, P., Vornlocher, H.-P., & Aigner, A. (2010). Polyethylenimine/small interfering RNA-mediated knockdown of vascular endothelial growth factor in vivo exerts anti-tumor effects synergistically with Bevacizumab. *The Journal of Gene Medicine*.

Hammond, S. M., Bernstein, E., Beach, D., & Hannon, G. J. (2000). An RNA-directed nuclease mediates post-transcriptional gene silencing in Drosophila cells. *Nature*, *404*(6775), 293–6.

Hennink, W. E., & van Nostrum, C. F. (2002). Novel crosslinking methods to design hydrogels. *Advanced Drug Delivery Reviews*, *54*(1), 13–36.

Hughes, J., Yadava, P., & Mesaros, R. (2010). Liposomal siRNA Delivery (pp. 445–459).

Kennedy, S., Wang, D., & Ruvkun, G. (2004). A conserved siRNA-degrading RNase negatively regulates RNA interference in C. elegans. *Nature*, *427*(6975), 645–649.

Kiel, J. W. (2010). *The Ocular Circulation*. *The Ocular Circulation*. Morgan & Claypool Life Sciences.

Kilickap, S. (2003). Bevacizumab, Bleeding, Thrombosis, and Warfarin. *Journal of Clinical Oncology*, *21*(18), 3542–3542.

Klein, M. L., Ferris, F. L., Armstrong, J., Hwang, T. S., Chew, E. Y., Bressler, S. B., …

AREDS Research Group. (2008). Retinal precursors and the development of geographic atrophy in age-related macular degeneration. *Ophthalmology*, *115*(6), 1026–31.

Kovach, J. L., Schwartz, S. G., Flynn, H. W., & Scott, I. U. (2012). Anti-VEGF Treatment Strategies for Wet AMD. *Journal of Ophthalmology*, *2012*, 1–7.

Kwatra, D. (2013). Drug delivery in ocular diseases: Barriers and strategies. *World Journal of Pharmacology*, *2*(4), 78.

Landfester, K. (2006). SYNTHESIS OF COLLOIDAL PARTICLES IN MINIEMULSIONS. *Annual Review of Materials Research*, *36*(1), 231–279.

Liu, B., Wang, Y., Zhang, M., & Zhang, H. (2016). Initiator Systems Effect on Particle Coagulation and Particle Size Distribution in One-Step Emulsion Polymerization of Styrene. *Polymers*, *8*(2), 55.

Lutty, G. A., Hasegawa, T., Baba, T., Grebe, R., Bhutto, I., & McLeod, D. S. (2010). Development of the human choriocapillaris. *Eye (London, England)*, *24*(3), 408–15.

Makino, A., Hara, E., Hara, I., Ozeki, E., & Kimura, S. (2014). Size Control of Core–Shell-type Polymeric Micelle with a Nanometer Precision. *Langmuir*, *30*(2), 669–674.

Meng, F., Hennink, W. E., & Zhong, Z. (2009). Reduction-sensitive polymers and bioconjugates for biomedical applications. *Biomaterials*, *30*(12), 2180–98.

Mousa, Adinoyi O. Garba, Mousa, & Adinoyi O. Garba. (2010). Bevasiranib for the Treatment of Wet, Age-Related Macular Degeneration. *Ophthalmology and Eye Diseases*, 75.

Ohno-Matsui, K., Yoshida, T., Uetama, T., Mochizuki, M., & Morita, I. (2003). Vascular endothelial growth factor upregulates pigment epithelium-derived factor expression via VEGFR-1 in human retinal pigment epithelial cells. *Biochemical and Biophysical Research Communications*, *303*(3), 962–7.

Pauleikhoff, D., Harper, C. A., Marshall, J., & Bird, A. C. (1990). Aging changes in Bruch's membrane. A histochemical and morphologic study. *Ophthalmology*, *97*(2), 171–8.

Pelton, R. (2000). Temperature-sensitive aqueous microgels. *Advances in Colloid and Interface Science*, *85*(1), 1–33.

Peppas, N. A., Bures, P., Leobandung, W., & Ichikawa, H. (2000). Hydrogels in pharmaceutical formulations. *European Journal of Pharmaceutics and Biopharmaceutics : Official Journal of Arbeitsgemeinschaft Fur Pharmazeutische Verfahrenstechnik e.V*, *50*(1), 27–46.

Pham, J. W., & Sontheimer, E. J. (2005). Molecular requirements for RNA-induced silencing complex assembly in the Drosophila RNA interference pathway. *The Journal of Biological Chemistry*, *280*(47), 39278–83.

Raemdonck, K., Demeester, J., De Smedt, S., Remaut, K., Sanders, N. N., Geest, B. G.

De, … Frechet, J. M. J. (2009). Advanced nanogel engineering for drug delivery. *Soft Matter*, *5*(4), 707–715.

Rajendran, L., Knölker, H.-J., & Simons, K. (2010). Subcellular targeting strategies for drug design and delivery. *Nature Reviews Drug Discovery*, *9*(1), 29–42.

Reischl, D., & Zimmer, A. (2009). Drug delivery of siRNA therapeutics: potentials and limits of nanosystems. *Nanomedicine: Nanotechnology, Biology and Medicine*, *5*(1), 8–20.

Runkle, E. A., & Antonetti, D. A. (2011). The Blood-Retinal Barrier: Structure and Functional Significance. In *Methods in molecular biology (Clifton, N.J.)* (Vol. 686, pp. 133–148).

Sanson, N., & Rieger, J. (2010). Synthesis of nanogels/microgels by conventional and controlled radical crosslinking copolymerization. *Polymer Chemistry*, *1*(7), 965.

Scherer, T. M., Leung, S., Owyang, L., & Shire, S. J. (2012). Issues and Challenges of Subvisible and Submicron Particulate Analysis in Protein Solutions. *The AAPS Journal*, *14*(2), 236–243.

Schmidt-Erfurth, U., Chong, V., Loewenstein, A., Larsen, M., Souied, E., Schlingemann, R., … Bandello, F. (2014). Guidelines for the management of neovascular age-related macular degeneration by the European Society of Retina Specialists (EURETINA). *British Journal of Ophthalmology*, *98*(9), 1144–1167.

Storkebaum, E., Lambrechts, D., & Carmeliet, P. (2004). VEGF: once regarded as a

specific angiogenic factor, now implicated in neuroprotection. *BioEssays : News and Reviews in Molecular, Cellular and Developmental Biology*, *26*(9), 943–54.

Sultana, F., Imran-Ul-Haque, M., Arafat, M., & Sharmin, S. (2013). An overview of nanogel drug delivery system. *Journal of Applied Pharmaceutical Science*, *3*, s95–s105.

Thakur, A., Fitzpatrick, S., Zaman, A., Kugathasan, K., Muirhead, B., Hortelano, G., & Sheardown, H. (2012). Strategies for ocular siRNA delivery: Potential and limitations of non-viral nanocarriers. *Journal of Biological Engineering*, *6*(1), 7.

Tokayer, J., Jia, Y., Dhalla, A.-H., & Huang, D. (2013). Blood flow velocity quantification using split-spectrum amplitude-decorrelation angiography with optical coherence tomography. *Biomedical Optics Express*, *4*(10), 1909.

Tugulu, S., Silacci, P., Stergiopulos, N., & Klok, H.-A. (2007). RGD—Functionalized polymer brushes as substrates for the integrin specific adhesion of human umbilical vein endothelial cells. *Biomaterials*, *28*(16), 2536–2546.

Tuo, J., Bojanowski, C. M., & Chan, C.-C. (2004). Genetic factors of age-related macular degeneration. *Progress in Retinal and Eye Research*, *23*(2), 229–249.

Van de Wetering, P., Schuurmans-Nieuwenbroek, N. M., Hennink, W. E., & Storm, G. (1999). Comparative transfection studies of human ovarian carcinoma cells in vitro, ex vivo and in vivo with poly(2-(dimethylamino)ethyl methacrylate)-based polyplexes. *The Journal of Gene Medicine*, *1*(3), 156–65.

Watts, J. K., Deleavey, G. F., & Damha, M. J. (2008). Chemically modified siRNA: tools and applications. *Drug Discovery Today*, *13*(19-20), 842–55.

Wert, K. J., Skeie, J. M., Davis, R. J., Tsang, S. H., & Mahajan, V. B. (2012). Subretinal Injection of Gene Therapy Vectors and Stem Cells in the Perinatal Mouse Eye. *Journal of Visualized Experiments*, (69).

Xia, H., Mao, Q., Eliason, S. L., Harper, S. Q., Martins, I. H., Orr, H. T., … Davidson, B. L. (2004). RNAi suppresses polyglutamine-induced neurodegeneration in a model of spinocerebellar ataxia. *Nature Medicine*, *10*(8), 816–820.

Yin Win, K., & Feng, S.-S. (2005). Effects of particle size and surface coating on cellular uptake of polymeric nanoparticles for oral delivery of anticancer drugs. *Biomaterials*, *26*(15), 2713–2722.

Zamore, P. D., Tuschl, T., Sharp, P. A., & Bartel, D. P. (2000). RNAi: double-stranded RNA directs the ATP-dependent cleavage of mRNA at 21 to 23 nucleotide intervals. *Cell*, *101*(1), 25–33.

Zetterlund, P. B., Kagawa, Y., & Okubo, M. (2008). Controlled/Living Radical Polymerization in Dispersed Systems. *Chemical Reviews*, *108*(9), 3747–3794.